Progress in Energy and Combustion Science 38 (2012) 818–845

Contents lists available at SciVerse ScienceDirect

Progress in Energy and Combustion Science

journal homepage: www.elsevier.com/locate/pecs

Review

Soot formation in high pressure laminar diffusion flames

Ahmet E. Karataş*, Ömer L. Gülder

Institute for Aerospace Studies, University of Toronto, 4925 Dufferin Street, Toronto, Ontario M3H 5T6, Canada

ARTICLE INFO

Article history:
Received 9 October 2011
Accepted 26 April 2012
Available online 30 June 2012

Keywords:
High pressure soot formation
High pressure combustion
Laminar diffusion flames
Soot diagnostics

ABSTRACT

The details of the chemical and physical mechanisms of the soot formation process in combustion remain uncertain due to the highly complex nature of hydrocarbon flames, and only a few principles are firmly established mostly for atmospheric conditions. In spite of the fact that most combustion devices used for transportation operate at very high pressures (e.g., aircraft gas turbines up to 40 atm, diesel engines exceeding 100 atm), our understanding of soot formation at these pressures is not at a desirable level, and there is a fundamental lack of experimental data and complementary predictive models. The focus of this review is to assess the experimental results available from laminar co-flow diffusion flames burning at elevated pressures. First, a brief review of soot formation mechanisms in diffusion flames is presented. This is followed by an assessment of soot diagnostics techniques, both intrusive and non-intrusive, most commonly used in soot experiments including the laser induced incandescence. Then the experimental results of soot measurements done at elevated pressures in diffusion flames are reviewed and critically assessed. Soot studies in shock tubes and in premixed flames are not covered. Smoke point fuel mass flow rate is revisited, and shortcomings in recent measurements are pointed. The basic requirements for tractable and comparable measurements as a function of pressure are summarized. Most recent studies at high pressures with aliphatic gaseous fuels show that the soot yield displays a unified behaviour with reduced pressure. The maximum soot yield seems to reach a plateau asymptotically as the pressure exceeds the critical pressure of the fuel. Lack of experimental data on the sensitivity of soot morphology to pressure is emphasized. A short summary of efforts in the literature on the numerical simulation of soot formation in diffusion flames at high pressures is the last section of the paper.

Contents

* Corresponding author. Tel.: +1 416 667 7700; fax: +1 416 667 7799.
E-mail address: emre.karatas@utoronto.ca (A.E. Karataş).

0360-1285/$ – see front matter © 2012 Elsevier Ltd. All rights reserved.
doi:10.1016/j.pecs.2012.04.003

1. Introduction

For reasons of optimal efficiency and size, combustion in practical gas turbine and reciprocating engines is turbulent and takes place at elevated pressures. The latter greatly increases the combustion intensity (energy released per unit volume) which scales with the square of pressure. On the other hand, the pressure has a significant effect on the overall soot yield as well as on the rates of soot production and oxidation in diffusion flames. But the experimental study of soot formation processes in turbulent diffusion flames at elevated pressures is not trivial. Reliable measurements of spatially and temporally resolved soot concentrations and oxidation rates in unsteady turbulent flames with shorter residence times are not usually tractable, especially at elevated pressures, whereas such measurements are relatively easy in laminar diffusion flames. As a consequence, most of the soot measurements are made in laminar diffusion flames that provide easily controlled conditions and the results can be projected to practical turbulent flames using the approximate approaches like the flamelet hypothesis. Experimental research in laminar diffusion flames under elevated pressures have been held back by the complications in designing an experimental apparatus and in operating instruments that require accessibility for intrusive and non-intrusive measurement techniques. In addition, the stability of laminar diffusion flames, especially originating from buoyancy effects, becomes an important issue at elevated pressures due to the increase in Grashoff number which scales with the square of pressure. These impediments have limited the number and the extent of experimental soot studies in laminar diffusion flames at elevated pressures.

Emissions of pollutants from transportation systems and in particular from propulsion systems constitute a relatively smaller portion of the global emissions; however, when the effects due to emission locations are taken into account, it is seen that they pose a more important threat on humanity than that would have been expected from considering their share only. Soot particles, for example, depending on where they are emitted can cause several different problems. Since Aristotle recognized candle smoke as a serious threat to pregnant women [1], our understanding of the detrimental health effects of soot and the mechanisms that are involved has improved considerably [2–10]. Today, human exposure to the urban sources of soot is seen as a big burden on the public health system. The resultant public awareness of air pollution problems and following green initiatives convinced governments to pass legislations such as the Clean Air Act [11] and the following significant amendments [12,13] in the United States, Directives on Ambient Air Quality [14] in the European Union, the Environmental Protection Act [15] in Canada, and similar measures in other countries.

Soot particles that are liberated in the upper atmosphere from aircraft engines affect the global thermal balance either by absorbing sunlight [16,17], or by contributing to contrail formation [18–22], or by depositing on highly reflective surfaces on earth [23,24]. The critical point beyond which the thermal stability of the planet may not be restored is believed to be reached in the near future. In this respect, as a short-term-focused solution to help in slowing the global warming, curbing soot emissions by improving our understanding its formation mechanisms can buy some time before larger-scale solutions can be implemented [25]. Such an approach is meritorious, especially when considering that emission of soot is not necessarily intrinsic to combustion, a phenomenon that probably could had not been more beautifully described than it was in the six lectures, titled “The Chemical History of a Candle”, delivered to a juvenile auditory at the Royal Institution of Great Britain during the Christmas Holidays of 1860–1. In the second lecture, Michael Faraday is known to state that [26] “The heat that is in the flame of a candle decomposes the vapor of the wax, and sets free the carbon particles; they rise up heated and glowing as this now glows, and then enter into the air. But the particles, when burnt, never pass of from a candle in the form of carbon”. He continues in the sixth lecture “You remember that when a candle burns badly, it produces smoke; but if it is burning well, there is no smoke… so long as the smoke remains in the flame of the candle and becomes ignited, it gives a beautiful light, and never appears to us in the form of black particles”.

Soot formation and destruction processes are affected by the environment in which they occur. Pressure is one of the environmental parameters that has a direct impact on the rates of these processes. In many cases, the overall combustion intensity in an energy conversion device scales with the square of the combustion pressure. Operating pressures in aircraft gas turbine combustors could reach 20 atm in civilian aircraft and 40 atm in military aircraft. The increase in the compression ratio has been steadily climbing since the first gas turbine engine built in mid 1930s, from about 5 to about 40 at the beginning of this century [27]. In diesel engines, pressures could exceed 100 atm routinely depending on the compression ratio and power generated. In space-related applications such as liquid rockets, pressures have come a long way from 5 atm in 1920s when Goddard invented the first liquid propellant rocket to over 250 atm in the course of history [28]. From a thermodynamic point of view, increasing compression ratios (leading to higher operating pressures) lead to higher thermal efficiencies. The overall reaction rate in hydrocarbon–air combustion (i.e., combustion intensity or heat release per unit volume) is roughly proportional to the square of the pressure: the relative size of the combustion device gets smaller as the operating pressure is increased for a required power output. These trends are expected to continue as overall fuel efficiency has become one of the major concerns.

Turbulent combustion is the *modus operandi* in most practical diffusion combustion systems and fires. However, the high level of intermittency and short levels of residence times involved in these flames make it difficult to track combustion events such as soot formation. The non-homogeneous nature of turbulent diffusion flames makes it challenging to isolate parameters that affect soot formation and oxidation. One of the most widely used approximations to exploit similarities between laminar and turbulent diffusion flames is to use the laminar flamelet concept, which provides a tractable flame model [29–31]. Conversely, more-easily controlled experiments are performed in rich premixed flames and

shock tubes. It is argued [32] that in premixed flames and in shock tube experiments, conditions may be quite different than those in the diffusion flame combustion.

On the one hand, premixed flames cannot simulate the very rich pyrolysis region where soot growth takes place in diffusion flames, and the shock tubes have very short residence times compared with diffusion combustion systems [33], although the shock tubes provide clean boundary conditions suitable for numerical simulation. On the other hand, it is believed that the chemistry involved in soot formation has the same character in both premixed and diffusion flames mainly due to the similar chemistry of soot formed in both cases. However, the soot precursor formation through fuel decomposition in premixed flames is competing with oxidative attack on these precursors, whereas in diffusion flames no such attack occurs on precursors produced as a result of the fuel pyrolysis [32]. In premixed flames, the soot formation rates are reduced with increasing flame temperature because of the fact that oxidative attack on precursors increases faster than the precursor formation rate, whereas in diffusion flames, increasing flame temperatures enhance the soot formation rates through enhanced pyrolysis reactions in the absence of oxidative attack [32,34]. Further, flame turbulence should not affect soot formation in premixed combustion; however, in diffusion flames, increasing turbulence reduces the soot formation rates by turbulent mixing and hence reducing the residence time of the pyrolysing fuel packet in a flamelet.

In shock tube pyrolysis experiments, the pyrolysis processes and subsequent soot formation take place at relatively constant temperatures and pressures, and the residence times involved are in the order of several milliseconds, whereas in diffusion flames residence times are measured as several tens of milliseconds. Also, in diffusion flames, the temperature-time history of a fuel element going through pyrolysis, soot precursor and nuclei formation, growth, and agglomeration varies and is not constant as in shock tube experiments [32]. It should be emphasized that, in view of the above discussion, one should be extremely cautious in projecting or applying results and trends obtained in premixed flames and shock tube experiments to diffusion flames.

1.1. Experimental challenges in studying soot formation at high pressures

Soot formation and oxidation processes are highly dependent on the flame environment in which they occur. If changes in flame environment disrupt the balance between the rates of these two competing processes, resultant changes in the soot properties and concentration, in turn, would have a significant effect on the flame and flow properties. This two-way interaction and the interdependence of the properties of fluids through the equation of state (e.g., pressure and temperature) does not permit to treat each potentially influential factor as an independent variable. Further, the high level of intermittency and non-homogenous nature in turbulent flows make diffusion flames intractable for detailed measurements (e.g., time-resolved) required to understand soot formation and oxidation properties [29,35,36]. Currently, measurements of spatially and temporally resolved turbulent mixing rates in sooting turbulent diffusion flames are not feasible. In addition, pressure compounds the problem further by not only affecting the soot formation and oxidation rates (mainly through changing time scales), but by also altering the turbulence field, which modifies the mixing rates. Through the use of approaches like flamelet hypothesis, which proposes that turbulent flames are a collection of deformed laminar flames, the similarities between laminar and turbulent flames could be exploited [37]. This opens the possibility of using laminar diffusion flames in high pressure experiments for tractable measurements. However, depending on the burner type used, i.e., co-flow, opposed jet, or Wolfhard-Parker, there are several difficulties involved in laminar diffusion flame experiments at high pressures.

The major complication originates from designing the experimental apparatus and from choosing the optimal measurement technique, intrusive or non-intrusive. One of the earliest high pressure rigs for laminar diffusion flame studies is shown in Fig. 1 [38]. Adopting intrusive techniques poses a greater challenge than using optical techniques as in most cases pressure chamber allows extremely restricted physical access to the flame. Even if an apparatus for the purpose of flame probing had been developed, due to the vulnerable nature of the flow, especially in an enclosed space at high pressure, the flow most probably would have been disturbed easily, and as a result, recirculation zones and turbulent regions could have appeared. Another problem in the implementation of intrusive techniques in high pressure combustion is related to the changes in the reaction rate and diffusion rate. As pressure increases, gaseous molecules become more closely packed, and thereby, the probability of a collision increases. At the same time, molecular diffusivity of the particles decreases. The former leads to higher reaction rates, but diffusion rate does not change much due to the counterbalancing action of increased densities of reactants: reactants that diffuse into the flame region are consumed at a higher rate, and as a result, the thickness of the flame reaction zone reduces as pressure increases [38,39]. To maintain a meaningful spatial resolution, probe size should be scaled with the flame thickness. However, this is not always feasible because small probes can easily be clogged at the orifice or turning points by soot build up.

In addition, due to higher gradients of temperature and soot concentrations, along with higher soot loadings at elevated pressures, the non-intrusive measurement techniques that have been

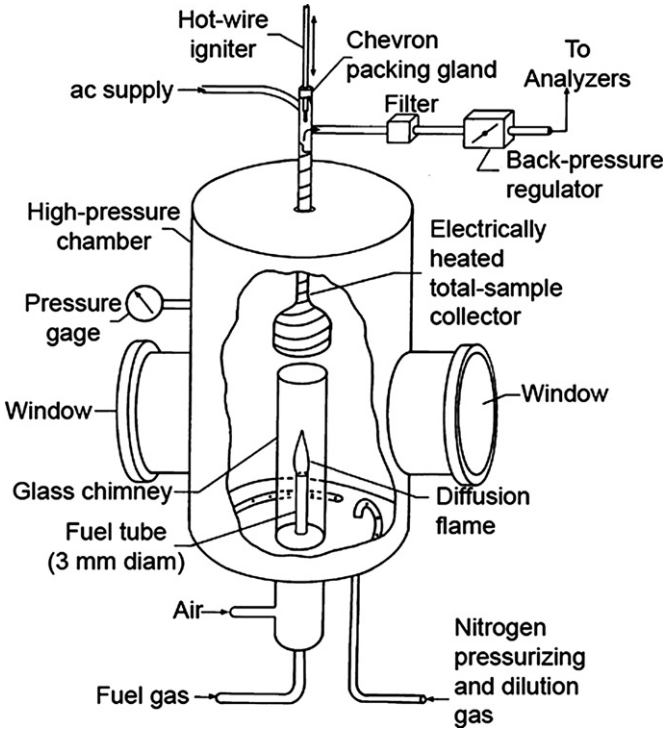

Fig. 1. Schematic diagram of the high pressure rig for laminar diffusion flame studies, Miller and Maahs [38]. Laminar diffusion burner and the sample collection system are indicated.

successfully used for atmospheric flames may not be easily adopted to high pressure conditions. The challenge can be better appreciated considering the example that the maximum soot volume fraction was found to increase from 14 ppm at 10 atm to 180 ppm at 60 atm for a co-flow laminar diffusion flame of methane–air [40]. Then, one realizes that the diagnostics system should be capable of measurements at a wide dynamic range in order to operate throughout the entire pressure spectrum of practical importance. This situation is partly improved by the use of lasers in combustion diagnostics and by the recent advances in sensor technologies. The enormous change in soot loading is only part of the problem; one has to look at other aspects as well. For example, underlying principles of some optical measurement techniques of soot may prove unreliable at high pressures, and this probably goes overlooked unless changes in the soot morphology such as primary particle size are considered. Another limitation of some optical measurement techniques is that they should rely on the flame itself (e.g., soot radiation) and thereby need not require seeding of the flow as this could easily interfere with the laminar flame structure. This prevents, for example, the use of particle image velocimetry (PIV) for flow-field measurement in laminar diffusion flames.

Further, a number of other problems arise from higher soot loadings at elevated pressures. Design of a burner and the choice of the material are complicated by the enhanced heat transfer to the burner nozzle due to radiation from soot. It was observed that high soot loadings under high pressure might congest the tip of the burner due to formation of crust-like solid carbon, clinging to the burner periphery of a co-flow burner [41–44]. For the same reason, care must be taken when porous or matrix structures are used inside the burner mouth as it was reported that soot particles tend to accumulate in the pores as pressure increases [45]. Higher soot loadings at elevated pressures are observed because soot formation in a flame is promoted at high pressure. The change in oxidation cannot always pace up with the increase in soot formation; at a critical pressure, flames start to smoke, i.e., soot particles are liberated from the flame. Smoking flames are not desired because in a pressure chamber, where even combustion products like water vapour are troublesome, soot can deposit on the optical ports or may deteriorate the pressure regulation mechanism of the vessel. Higher soot loadings combined with the changes in the flame structure lead to higher temperature gradients [46], which mean higher density gradients. One difficulty associated with high temperature gradients is beam steering—the change in the direction of the light passing through a medium of non-homogeneous refractive index induced by density gradients. This problem is worsened by the need to use thick quartz windows in the optical ports of the pressure vessel.

Possibility of explosions is a serious concern in the design of high pressure combustion vessels and should be addressed carefully. As pressure increases, flames are more prone to flashback, a hazardous condition that originates from flame propagation upstream through the fuel nozzle. Diffusion flames have an inherent advantage over premixed flames in resisting flashback [42] since the reaction rate is controlled by the rather slow rate of diffusion than the rate of chemical reactions. As noted in [37], not many comprehensive experimental studies have been conducted on high pressure laminar diffusion flames as a result of these complications. Most of the high pressure experiments report flame shapes, smoke points, and (often limited) temperature field and soot concentration measurements.

It seems that opposed jet and co-flow laminar diffusion flames are best suited for high pressure experiments. However, there might be some issues in opposed jet flames for tractable soot measurements, although these flames have been successfully used for ignition, extinction, and strain for sooting limits at above atmospheric pressures [47,48]. The effect of strain rate, K, on soot formation makes it impossible to single out the intrinsic effect of pressure in the counterflow configuration. Increasing strain rate can curb the formation of incipient soot particles [49]. The residence times are not comparable at different pressures, and as strain rate increases, flame thickness reduces (flame thickness $\propto K^{-0.5}$ [50,51]). Moreover, counterflow flame temperature is also affected mostly due to changing amounts of reactant supply into the flame and to changing residence times [51,52]. More importantly, the usual practice of maintaining momenta at fuel and air sides equal in counterflow experiments does not allow keeping track of mass flow rate of fuel consumed by the flame sheet. Due to high stoichiometric ratios, there usually is a great amount of excess fuel, which is not involved in combustion but may affect temperature and contribute to precursor formation. For these reasons, it is not surprising that the most widely used flame has been the co-flow diffusion flame for soot-related studies at elevated pressures [38,40,43,44,46,53–65].

1.2. Tractability and laminar co-flow diffusion flames

The tractability of the laminar co-flow flames at elevated pressures is based on the premise that the flame heights are independent of pressure, that is, if the fuel mass flow rate is fixed, and if the flame is buoyancy dominated. Pressure independence then could only be possible if the flame cross-sectional area scales with the inverse of the pressure [32]. The inverse dependence of the flame cross-sectional area on pressure implies that the residence times are independent of the pressure, and measurements can be compared at the same heights above the burner exit. This can be illustrated simply as follows: it is shown that, to a first approximation, the height of a buoyancy dominated laminar co-flow diffusion flame, established on a circular fuel nozzle, scales with molecular diffusivity, D, and fuel flow rate, Q, as [66],

$$H \propto \frac{Q}{D} \propto \frac{1}{P}\frac{\bar{v}A}{D} \tag{1}$$

for a fixed flow rate of fuel. Here, $\bar{v}$ is the mean fuel exit velocity and A is the fuel nozzle exit area. Since molecular diffusivity is inversely proportional to pressure, P, i.e., $D \propto 1/P$, then the height of the diffusion flame is independent of the pressure. At a given height above the burner nozzle exit, the average velocity within the flame envelope does not change with pressure, if the flame cross-sectional area varies inversely with pressure. That is, as pressure increases, the material flow within the flame envelope will be through a narrower cross section but at a higher density, thus keeping the average velocity constant at a given height. This argument assumes that the air entrainment into the flame envelope does not change much with pressure. The first experimental verification of pressure independence of flame height for co-flow flames, albeit within a limited pressure range of 1–1.5 atm, is in the seminal study of diffusion flames by Burke and Schumann [67] in 1928. Visible flame heights of methane–air flames up to 100 atm are shown in Fig. 2 [68]; it is apparent that flame cross-sectional area decreases with pressure, and flame heights are almost constant at all pressures.

It should be noted here that soot processes have differences within buoyant and nonbouyant laminar diffusion flames. Local effects of buoyancy are limited in the soot reaction zones of practical turbulent flames, and nonbuoyant laminar diffusion flames are more representative of soot processes in non-premixed turbulent flames. For this reason, when projecting buoyant laminar diffusion flame results to practical turbulent flames, the differences between buoyant and nonbouyant flames should be taken into account. It is

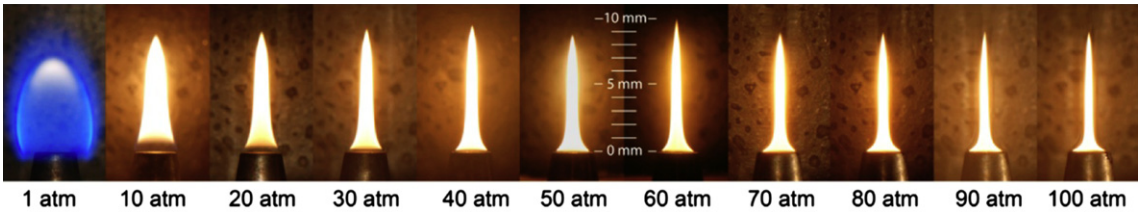

Fig. 2. Pictures of laminar methane–air co-flow diffusion flames from atmospheric pressure to 100 atm. Methane flow rate is constant at 0.55 mg/s [68].

not trivial to establish nonbuoyant laminar diffusion flames in laboratories on Earth to study the effect of pressure. Zero gravity laminar diffusion flames experiments at elevated pressures are not available yet because of the cost and safety issues associated with high pressure flames on spacecraft. Drop towers and aircrafts flying parabolic trajectories do not provide microgravity long enough for high pressure experiments.

It is not clear how co-flow diffusion flames attach themselves to the burner nozzle, and flame attachment and stabilization have been actively investigated at atmospheric pressure [69–75]. The general belief is that a premixed region that is created in the wake of the burner nozzle periphery plays a catalyst role in flame attachment. Heat and radical absorbtion by the fuel nozzle inhibits any chemical reaction around its vicinity [76], and expansion from both sides of the fuel nozzle enhances mixing. As expected from the interdiffusion of the reactants, the equivalence ratio, φ, inside this premixed zone varies [77]. Experiments at atmospheric pressure support the presence of a premixed zone at the burner rim as this region is usually observed blue. It is becoming more clear that this region harbours a unique triple flame, a tribrachial flame structure, consisting of a rich premixed flame, a lean premixed flame, and a diffusion flame [70,72,75]. Observations at extreme pressures however cast doubt on the applicability of this description to all pressures. Experiments at super-atmospheric pressures [40,46] show that the blue region diminishes as pressure is increased, and the region is soot laden, and as the ambient pressure approaches to zero, flames are not anchored at the burner rim and under certain conditions are more-easily lifted [78]. Even though a complete understanding of flame stabilization is lacking, co-flow flames are still known for their robustness. Yet, some stability issues have been observed at high pressures [68], especially working with the vapours of liquid fuels [79,80]. It is believed that due to the thinner reaction zone at above atmospheric pressures, the reactant flow mechanism cannot as easily make up for the effect of the slightest disturbance [38].

1.3. Soot formation mechanism

The formation of soot is a rather complex process, an *evolution* of matter in which a soup of elemental molecules undergo several simultaneous reactions where sophisticated structures consisting of millions of carbon atoms are formed within a few milliseconds. Throughout the process, interaction of chemical kinetics, heat and mass transfer, and fluid flow complicates the situation further. Even though how the soot particles and their precursors are formed in flames is a matter of intense debate, and not many fundamental aspects of soot formation have been firmly established, the literature on soot formation is very extensive. There are a number of reviews on soot formation mechanisms in combustion literature. In most of them, no distinction is made between premixed and diffusion flames, see e.g., [81]. For completeness, a brief review and discussion of soot formation relevant to laminar diffusion flames is presented in this section. Most soot studies are done in flames (either premixed or diffusion) and in shock tubes. A typical characteristic time scale of soot formation is tens of milliseconds in flames, whereas behind the reflected shocks, it is several milliseconds. Electron microscope analysis of soot collected from flames suggests formations of clusters of fractal-structures, called agglomerates, with tens hundreds of primary particles attached. Primary particles, if nascent, may differ in structure with a liquid-like look and show bi-modal size distribution with diameters as small as few nanometers [82,83]. Mature particles are almost spherical with diameters ranging from several nanometers to about 50 nm or larger [84,85]. Most soot agglomerates may contain several hundred or more primary particles. The transmission electron microscopy (TEM) studies show that the primary soot particles have a layered structure and consist of numerous concentric crystallites; the degree of order, rearrangement of the amorphous regions into crystallites, depends on how much annealing soot particles undergo [86]. A primary soot particle contains on the order of 10^3 crystallites, each as thick as 1.2 nm [87]. Crystallites are composed of stacks of binary arrays of carbon atoms (typically, 2 to 5 binary arrays). These pairs of carbon arrays are commonly described as platelets. Each array is in the form of a hexagonal lattice, and two arrays are arranged face-centered in dual configuration to form a platelet. The pair spacing is only slightly larger than that of graphite with a value of 0.355 nm [87]. Particles produced in flames and sampled are quite different from those formed in the exhaust gases [88]. Young soot particles can contain equal number of hydrogen atoms as carbon atoms and high concentrations of PAH residuals. As soot particles mature, they undergo structural reorganization and dehydrogenation and/or graphitization processes after which hydrogen content reduces to 0.1 or even less. An empirical composition formula of C_8H was proposed for soot [84]. However, differences in the composition of soot produced through different processes usually do not show up in the morphological structure, but in the dynamics of agglomeration [88].

Several different types of species have been suggested as the key gaseous precursors of soot—polyacetylenes (polyynes), neutral free radicals, ionic species, common precursors with fullerenes, and polycyclic aromatic hydrocarbons (PAHs). Recent studies stated that the PAHs are the most probable soot precursors [89–99]. Several authors have suggested that particle inception occurs through the formation of aromatic-aliphatic-linked hydrocarbons or PAHs with five-rings (see, e.g., [100]), which later graphitize forming more compact structures. The homogeneous inception of large molecular precursors is still an incompletely studied area. The soot particle size increases in reactions of surface growth by the active sizes on the particle surface. Coagulation forms larger particles, where during agglomeration, the primary particles stick to each other, forming chain-like aggregates.

The primary focus of research in gas-phase kinetics of soot precursor formation is on the formation of the first aromatic ring from small aliphatics since this step is considered to be the bottleneck to the formation of higher PAH [101–107], although

there are still uncertainties about the identity of final chemical precursor(s) and the stage at which they start to coalesce. The widely believed mechanism is that the gaseous precursors that coagulate into soot particles are PAHs [32,108–111]. The rationale for this view is based on the observations that the PAHs bridge the gap between hydrocarbon fuel and the soot, and the chemical structure of soot is similar to PAH on an atomic level [112]. The uncertainties are (a) the identity of the gaseous precursor(s); (b) the chemical kinetics of formation of the precursor(s); (c) the stage at which precursors form into soot and the form soot takes [113]. In several studies, pyrene was proposed as the final gaseous precursor [113–116], whereas in some others coronene (300 amu) was favoured as the final precursor [117]. In addition, in some recent soot formation studies, heavier PAHs larger than coronene have been observed, and it was argued that whether it is more plausible to think of a coagulation mechanism that forms first soot particle (about 2000 amu) from heavier PAHs rather than coronene [95,99,118,119].

One of the widely known mechanisms for the formation of the first benzene ring is the hydrogen-abstraction-carbon-addition (HACA) mechanism [107,111]. It is a kinetics scheme which involves addition of acetylene to n-C_4H_5 to form benzene [101,120–122]:

$$\text{n-}C_4H_5 + C_2H_2 \rightleftarrows C_6H_6 + H \tag{2}$$

Several studies found this mechanism as the dominant one in PAH formation [99,118,119,122], although some recent work claimed that the rate of increase in PAH by HACA is not sufficient enough to account for the rapid formation of soot [105,116–128]. In contrast to this, the even-carbon-atom pathways, several odd-carbon-atom pathways have been suggested; one of the widely known ones involves the propargyl radical [129,123–131]:

$$C_3H_3 + C_3H_5 \rightleftarrows C_5H_4CH_2 + H + H \tag{3}$$

Propargyl radical recombination is claimed to be the dominant mechanism in many flames [132,133]. The reaction pathways can be summarized as [133]:

$$C_3H_3 + C_3H_3 \rightleftarrows \text{benzene} \tag{4}$$

$$C_3H_3 + C_3H_3 \rightleftarrows \text{fulvene} \tag{5}$$

$$C_3H_3 + C_3H_3 \rightleftarrows C_4H_5C_2H(\text{2-ethynyl-1,3-butadiene}) \tag{6}$$

$$C_3H_3 + C_3H_3 \rightleftarrows C_6H_5(\text{phenyl}) + H \tag{7}$$

The mechanism of soot precursor formation by aromatic radical–radical combinations and radical–molecule reactions was discussed in [81,111,134,135]. These mechanisms, or their variations, seem to be the main contenders, and even in a given flame, more than one of them could be playing a role. In some flames, none of these simple reactions can fully explain precursor formation [136].

The formation of single-aromatic-ring compounds is a very common area of investigations, but it may not be the rate-limiting step [111,137]. It was suggested that the growth of higher PAH can be initiated by the direct formation of multi-ring PAH, bypassing the formation of the benzene ring [111]. Such alternative proposal includes also the formation of aromatics from condensation of polyacetylenes $C_{2n}H_2$ [138], combination of C_4H_X species [139], as well as combination of larger radicals [99,140]. Kazakov et al. [141] showed that the formation of the first aromatic ring via reactions of C_6H_X species as well as the ring–reactions plays a significant role with increasing pressure. Such reactions were considered in many kinetic mechanisms [97,102,107,142,143]. Growth of aromatic species by HACA mechanism [104,111,144–146] and through the mechanism in which hydrocarbons with conjugated structures and their derivatives are critical intermediates to PAH growth and soot nucleation [127,147] are the two schemes that operate via hydrogen atom migration and migration reactions [147,148]. In the molecular level, PAH–PAH binding adds the third dimension to the molecules [149], and in the particulate level, PAH–soot collisions contribute to the accumulation of mass into the soot [150].

Emissions of soot from a combustion device or from a laboratory flame depend on the competition between the soot formation and soot oxidation. Therefore, the process parallel to the aromatics growth is the oxidation of aromatics and soot. The hydroxyl radical was considered as the primary oxidizing agent of soot particles [108,151–153]. On the other hand, at least in laminar diffusion flames, molecular oxygen was proposed to be the main player in aromatics oxidation [111]. As in the case of PAH and soot formation, the detailed descriptions of PAH and soot oxidation are still elusive, and only certain aspects of these phenomena have been established.

The very brief discussion of the soot formation and oxidation given above indicates that the state of the art is not yet at a level to be able to achieve sound predictions of soot formation and oxidation in flames from the first principles using numerical simulation. The main drawback is that not all elementary reaction rate coefficients are available [154]. Current approaches to modeling soot processes in combustion can be crudely classified as [155]: (a) purely empirical correlations and models, (b) semi-empirical approaches involving solutions of soot formation and oxidation reactions (not necessarily elementary reactions, but lumped or global reactions), and (c) detailed models that solve the rate equations for elementary reactions that lead to PAH and soot. Once the soot nuclei appears (i.e., soot inception), the next steps are in the "particulate" phase involving surface growth, coagulation, and agglomeration in parallel with soot oxidation. It is believed that surface growth, which is similar to HACA reactions in the molecular level [111], is the stage in which significant amount of molecular mass condenses into the soot particle and eventually makes up most of the final mass [156].

Homogeneous soot particle inception can be considered to be a process of physical condensation or a process of chemical (reactive) condensation. In physical condensation process, the supersaturation of macro-molecular precursors generated by gas-phase reactions become sufficiently high, and as a result, the partial pressure of the precursors forces the macromolecules to condense physically into liquid-phase soot [157,158]. The homogeneous condensation can be approximated by classical nucleation theory, which gives the number of critical nuclei per unit volume [158,159]. The chemical (reactive) condensation, on the other hand, considers the process of continuous reactions of macro precursors as the driving mechanism of homogeneous soot particle inception [110,126,146]. In the particulate phase, the growth, coagulation, and agglomeration could be modeled using the sectional model or method of moments, similar to approaches used in aerosol physics.

2. Diagnostics methods in soot studies

Improvements in combustion diagnostics and in particular soot diagnostics allowed more-detailed numerical simulations of flames and soot formation and better validation of the results of these simulations. Most of the advances are due to advancements in other branches of science. For example, the adoption of laser technology as a tool in soot diagnostics has been the biggest breakthrough. Design of the next-diagnostics methods requires multi-disciplinary thinking and awareness of the frontiers of several areas such as laser and sensor technologies and optics.

Methods of soot diagnostics are generally divided into two categories depending on the criterion of how flames are accessed: (a) Intrusive techniques are those that require physical probing of the flame, and (b) non-intrusive techniques, as the name suggests, rely on the measurements of the flame emission itself or the optical probing of the flame by an external light source, which makes use of various optical phenomena such as scattering. Most of the time non-intrusive techniques are preferable because of their versatility and non-interference with the flame. That being said, optical diagnostics usually fall short in studying soot morphology, even though it is not clear how well *ex-situ* measurements in methods employing physical collection of soot capture the true nature of the soot morphological structure in flames [160]. In many cases, intermittent nature of turbulent combustion, restricted physical or optical access, and spatial and temporal limitations raise problems regardless of the technique adopted. Main parameters of interest to soot studies are soot volume fraction and soot morphology (i.e., primary particle diameter, aggregate properties, etc.). The interpretation of these measurements greatly benefits from the knowledge of basic flame properties such as flame temperature, reaction rate, and reaction zone thickness, as well as gas-phase species concentration and flow-field.

2.1. Intrusive techniques

Combustion measurements using probes as a direct measurement device or as a tool to collect samples of the flow have been extensively done and are well established. Probing techniques are employed with some success in the measurement of nearly every parameter of interest, i.e., pitot tubes for velocity measurements, thermocouples and pneumatic probes for temperature measurements, and various types of isokinetic and sonic probes for species concentration measurements [161]. A probe method can be *in situ* as in the case of thermocouples or *ex situ* as in soot morphology studies by probes, which require the collection of soot particles and a subsequent analysis outside the flame using relevant diagnostics systems. The success of probing techniques lies in the simplicity and ease of use of probes and often their being a cheaper alternative to optical instrumentation. This is of course at the expense of higher intrusiveness of physical probing in comparison with optical probing: stagnation of the flow due to insertion of an obstacle, a probe, creates more of a disturbance to the flow, reaction, etc. than would often be caused by the light passing through, a disturbance in the forms of heating the flow, energizing the molecules, etc. [161]. Even though fluidic disturbances are partially prevented by tapered probe designs and by the advances in materials science and manufacturing techniques that gave way to micro probes with no need for cooling as often a better alternative to massive probes with water cooling, other problems are present such that probes may affect spray dynamics in an engine or may disturb flame dynamics serving as a flame holder [162]. Nevertheless, under the most careful experimental conditions, it was demonstrated using probing methods that main species mass fractions and velocity in a turbulent flame can be measured within 10% and temperature within 5% of their turbulence-averaged means [162]. The accuracy is much worse in the case of measuring radicals and minor species, e.g., significant disparities were observed for the measurement of nitric oxides by optical methods and probe-sampling methods [163].

Probe-sampling methods are also used to collect particulates inside a flame or an exhaust. Smoke opacity measurement method is commercialized and used for the enforcement of legislations on soot emission. It usually accompanies the roadside visual inspection, and if deemed necessary, often a standardized test procedure [164] is followed. This involves the probe placed at the exit of a vehicle exhaust pipe in a specified way and subsequent measurements of smoke opacity by the light extinction principles. Gas turbine manufacturers took a slightly different approach to measure smoke levels during the engine design and development phase. As specified by the Society of Automotive Engineers [165], the post engine stream is probed, and this flow is directed towards a standard filter cartridge. Quantitative results are obtained from the analysis of the change in the transparency of the filter. This technique was the norm in smoke certification three decades ago [166], even though optical methods have mostly superseded intrusive techniques where the advantages overweight and where enough resources are available. Most recently, the efforts of measuring particulates in the gas turbine exhaust have been focusing on emerging instruments including laser-based techniques [167,168].

Increasing awareness of the role of particle and aggregate size in assessing the toxicity of combustion-generated particulates brought about a need for fundamental studies in soot morphology. Probe collection techniques in combustion science are various, each having own strengths and shortcomings. Therefore, some researchers used multiple probing techniques in their studies [82,169] or chose the probe that fits best to the flame configuration studied [170]. Under identical flame configuration, results obtained from using different probe designs do not always match [82,169]. This is partly because processes ongoing from the moment the sampling starts in a flame till the moment that the measurements are completed are fairly complex. The variances in the results of measurements by different probes may be due to different residence times or different probe characteristics that affect the flame processes concerning soot such as soot growth or to different thermophoretic forces and diffusion and heat transfer rates that exist in a probe, but usually a combination of all. As a result, soot particles measured by different techniques may exhibit differences in their structural orderliness, primary particle size, the arrangement of aggregates, and the number of particles per aggregate.

A particular sampling method has become the mainstay of studies on soot morphology such that most of the results in the combustion literature are to some extent comparable. In this method, a surface element (often a mesh) is attached to a probe, and the probe is immersed in the flame for a controlled duration [171]. Thermophoresis is the driving mechanism of soot deposition, and a short period of time (on the order of 30 ms) is often enough for adequate soot deposition. When temperature gradients are sufficiently large at the scale of typical aerosol diameter, the difference in the kinetic energies of the molecules at opposite sides of an aerosol particle repel the particle towards the lower temperature, and this is the case when a cold probe is immersed inside a flame [171]. This method is superior in the sense that the deposition is in the flame, and many intermediate steps between the probing and diagnosis are eliminated. The relatively cold surface of the probe helps in slowing down processes that affect soot morphology, and what's more, the mesh material can be chosen as one that is a chemical inhibitor. The samples are examined for their morphology often under a transmission electron microscope, which is ideal for soot visualization as it can resolve primary particles in an aggregate as well as planar structures inside a soot particle. As a versatile method, thermophoretic sampling, together with electron microscopy, is utilized in the studies of various flame configurations, from diesel engines [172,173] to pool fires [174] and from lab-scale turbulent diffusion flames [175–177] to laminar diffusion flames [171,178–187]. Thermophoretic sampling and subsequent diagnostics were extended for soot volume fraction measurements [177,179]. This diagnostic technique has an advantage over optical techniques that soot optical properties such as refractive index are not required. In fact, it was used to

test the validity of the refractive index value presumed in the optical studies [177]. Practitioners of this method [177,179] claim that they were also able to diagnose nascent particles more efficiently because these particles interact less with the light, thereby go unnoticed in measurements using optical methods.

2.2. Non-intrusive techniques

Optical methods have gained much popularity in combustion community due to their mostly non-perturbing nature, even though non-intrusiveness is a matter of debate for techniques such as laser induced incandescence. However, the rule of thumb is that provided that the time interval between repetition of the measurements is larger than the convective timescales, the flow recovers between measurements. Optical techniques that deliver information on soot generally rely on the unique properties of soot in a flame. It is not uncommon that these techniques assume that all the optical phenomena taking place in a flame is only an outcome of the presence of soot, and the flame itself, devoid of soot, is transparent. Such an assumption is excellent for most of the electromagnetic spectrum of interest in a wide variety of sooting flame configurations. Therefore, use of these techniques is fairly common in combustion studies.

2.2.1. Light extinction technique

Light extinction technique is a widely used technique for measuring soot concentration in a flame. Light passing through an aerosol-laden region is partly absorbed by the aerosol particles, and the extent of extinction can be used to judge the abundance of soot particles in a flame. It is one of the simplest optical methods, yet very effective. One of the earliest implementation of the light extinction technique can be traced back to Faraday's lectures, where he placed a candle between an electric lamp and a screen [26]. He pointed out the extinction as "You observe the shadow of the candle and of the wick", and thereafter explained to the audience: "What we see in the shadow as the darkest part of the flame is, in reality, the brightest part".

The total amount of light extinction by a spherical particle can be expressed as the sum of the total absorbtion and the total scattering, the latter being the combination of diffraction, reflection, and refraction [188]. The total scattering Q is given by

$$Q = \frac{\pi^4}{4\lambda^4} d^6 f(m, N) \tag{8}$$

where λ is the wavelength, d is the particle diameter, and f is a function dependent on soot refractive index m and soot density N. The total absorption can be expressed in terms of absorption coefficient K_a as

$$K_a = \frac{\pi^2}{\lambda} E(m) N d^3 \tag{9}$$

where $E(m)$ is the soot refractive index function given by $E(m) = -\mathrm{Im}(m^2-1)/(m^2+2)$. Scattering scales with $d^6\lambda^4$ whereas absorption scales with $d^3\lambda$. Therefore, the relative contribution of scattering and absorbtion to extinction depends on the non-dimensional scattering parameter, the ratio of the perimeter of the particle projection to the wavelength of the incident light. In the regime where particles are relatively small compared to radiation wavelength (scattering parameter smaller than 0.3), namely the Rayleigh regime, light extinction due to scattering is negligible compared to light absorption by soot particles [188]. That is, when

$$\frac{\pi d}{\lambda} \leq 0.3 \tag{10}$$

it is seen that $K_a \geq Q$. A rough calculation shows that the limit of Rayleigh regime corresponds to green light for a particle of 50 nm diameter. However, as discussed in Section Section 1.3, soot is generally present in flames in forms of aggregate structures, which are neither spherical nor their equivalent geometry lies within the Rayleigh regime for visible light. Thus, techniques that measure light extinction and make use of Rayleigh simplification may slightly overestimate the soot concentrations.

Nevertheless, the technique is shown to have measurements at a wide range of wavelengths achieving noise levels less than 0.0007 in extinction and a spatial resolution of 30–40 μm for planar imaging [189]. In this implementation of light extinction technique, that is, the line-of-sight-attenuation technique (LOSA), an arc lamp was used to form a large beam of light that propagates through the flame. In other realizations, a laser source is used in place of the arc lamp. The intensity of light is measured with the flame and without the flame, and their ratio corresponds to the transmissivity of the flame. The transmissivity map can be computed at once by taking 2-D pictures of a collimated light source passing through the flame location in which every pixel corresponds to a discrete measurement, or can be constructed from consecutive measurements of a point source. In either case, the attenuation is line-of-sight averaged. Thus, this technique is not suitable for diagnosing turbulent flames. In the special case of axisymmetrical flames, local soot volume fraction can be obtained by the radial inversion of the 2-D data through a tomographic reconstruction algorithm.

Extinction techniques are scarcely used in soot studies at elevated pressures when it is desired to obtain radially resolved soot volume fraction. The advantages of light extinction are shadowed by the effect of beam steering. Beam steering is the deflection of light from its original axis because the medium acts as a lens in the presence of density gradients. In other words, refractive index field is not homogenous in a flame due to density gradients usually induced by temperature gradients. The situation only worsens at elevated pressures as the influence of temperature gradients is more pronounced. For example, at 10 atm, beam steering grows into the primary source of error in light extinction calculations of a co-flow diffusion flame [190]. Flame shrinkage and increasing radiative heat loss are some examples on how pressure affects beam steering, that is, density gradients are increased. For the same reason, light extinction technique is impractical for measuring soot volume fraction around a stagnation plane, e.g., for counterflow diffusion flames. Qualitatively, angular deflection was found to increase from below 1 mrad at atmospheric pressure to above 5 mrad at 10 atm for a co-flow diffusion flame [191], and it was found to climb to over 8 mrad at the stagnation region of a counterflow diffusion flame [192]. Beam steering at high pressures can be prevented to a certain extent through replacing the collimated light source with a diffuse light source, and satisfactory results were reported with this arrangement at 10 atm [190].

2.2.2. Spectral soot emission technique

Spectral soot emission (SSE) techniques depend on the radiation emitted from soot along a given chord. This technique provides a way of measuring soot volume fraction without the need for an illuminating light source. Emission and absorption measurements at a single wavelength, if available together, was shown to be adequate to obtain radially resolved values of temperature and soot concentration in an axisymmetric laminar diffusion flame when radial deconvolution is applied [193]. On the other hand, in order to obtain soot concentration by emission analysis only, emission measurements need to be done at multi-wavelength. The simplest implementation is the two-colour emission analysis of flames, and it was routinely used in comparison with absorption analysis [194–196]. Iuliis et al. [197] extended the method to multi-

wavelength measurements and achieved better agreement with the simultaneous light extinction measurements for a co-flow diffusion flame. Snelling et al. [198] refined the technique by assessing the limits of focus and by applying corrections to the measurements to compensate for the spectral soot emission lost prior to leaving the flame (loss is due to the peer soot particles). The implementation of two-colour spectroscopy can be broadened to asymmetric flame configurations by multi-angle imaging [199].

Spectral soot emission has been used numerous times in high pressure combustion studies [40,46,55,56,58,63]. This technique fits well to studies at elevated pressures because a dependence on soot radiation means that the accuracy of the results is increased when measuring higher soot concentrations, which are readily observed at higher pressures. An exception is extreme soot loadings, which optically thicken the flame so self-scattering and absorbtion cannot be overlooked. Another key advantage of spectral soot emission measurements is that it requires access to the flame through a single port, whereas diagnostics systems with an external light source requires a minimum access of two ports. As a result, a simpler pressure chamber design can be used, or remaining ports can be used for simultaneous measurements of different parameters.

2.2.3. Laser induced incandescence

Laser induced incandescence (LII) technique has come into prominence within the recent decades. In this technique, soot particles in a flame are heated to around/above their vaporization temperature along a line or plane by a short-duration high-fluence laser pulse. The energy that is transferred to the soot by the absorption of the laser light is partly released as quasi-blackbody radiation from soot within the few hundred of nanoseconds following the laser pulse. This incandescent broadband light is detected and analyzed further. The underlying principles are that the magnitude of the incandescence signal is proportional to soot concentration, and the profile of the temporally-decaying incandescence is related to the particle size distribution [200–202].

Even though underlying principles are fairly simple and of general validity, implementation of LII systems varies in complexity and success throughout laboratories and applications. Laser induced incandescence is unrivaled in the measurement of soot concentration in turbulent flames because high temporal resolution of this technique, which is only limited by the laser fire rate, can track down the changes in a turbulent flame. In other flame configurations, laser induced incandescence stands out for its high dynamic range; the system without any special modification can make credible measurements of extremely low and high soot concentrations. Further, errors that are involved during the tomographic inversion of the line-of-sight integrated measurements of soot are avoided since LII can be set to measure spatially-resolved local incandescence. Since incandescence is broadband blackbody radiation, in LII the detection window of wavelengths can be chosen with a greater flexibility to minimize any interference from other sources of emission in a flame.

Laser induced incandescence has seen extensive usage in studies of soot formation in the combustion of diesel sprays at high pressures either in simplified combustors [203–206] or in full-scale engines modified for optical access [205–208]. However, the effect of pressure in the combustion cell on the accuracy of LII measurements is still ambiguous for the greatest part. The effect seems to be systematic but discrete for different pressure intervals, which is determined by the pressure dependency of the mean free path [209,210]. There are three regimes, which separate the effects of the presence and absence of collisions and transitional effects, but these regimes differ in definition when the flow is aerosol laden. The non-dimensional parameter that shows the effect of rarefaction is constructed using the size of the aerosol particles rather than the molecular size as it is more of an interest to find out how the heat transfer between the aerosol and gaseous environment is affected [211].

At sub-atmospheric pressures, where collisional effects are less important, the pressure has a direct effect on the energy balance of the laser-heated particles. Following the absorption of the laser energy, soot undergoes a process of energy loss via sublimation, heat conduction, and radiation. Among these heat transfer mechanisms, radiation from soot is believed to be negligible in most flame configurations and relevant LII systems [200]. It is becoming clear that this is not the case for near vacuum conditions [212]. Liu et al. [213] formulated the heat transfer rate for the aforementioned mechanisms as a function of pressure and temperature for different primary particle sizes. In their analysis, radiation stands out amongst others when temperatures are reduced below soot vaporization temperature and when near vacuum is realized. This has serious implications on the LII signal. First of all, particles that glow longer due to diminishing heat conduction lead to lesser signal decay. If the LII analysis makes use of integrated signal rather than instantaneous signal in order to infer soot volume fraction, calibration of the LII system at a fixed pressure leads to the overestimation of soot volume fraction as pressure decreases in the free-molecular regime. Second, laser induced incandescence is further limited in low pressure combustion experiments because the underlying principles for measuring particle size distribution is usually built upon physics of heat conduction. Particle volume increases with the third power of the particle diameter, whereas particle sweep area is only proportional to the second power; thus, smaller particles with relatively higher number of collisions per unit particle volume lose their internal energy faster when collisional effects are present. Even though radiation heat loss is also a function of particle diameter, the change in particle internal energy and energy loss by radiation show identical dependence on particle diameter within the Rayleigh regime [212]. As a result, temperature decay rate provides no information on primary particle size when radiation is the only dominant heat transfer mechanism [212,213]. Nevertheless, particle size still retains its effect on the maximum particle temperature even within the Rayleigh regime [213].

The use of laser induced incandescence is even more problematic at elevated pressures. There have been few studies that delve into the effects of elevated pressures on LII measurements [209,210]. The difficulties have not precluded the efforts of using LII for studies of co-flow laminar diffusion flames at elevated pressures [44,214]. Uncertainties that arise from increasing pressure can be divided into those during experimentation, those during the analysis of the experimental data, and those during the calibration of the system.

Most of the problems during the experimentation stage is ironically due to the changing soot loadings inside a flame. Heavily sooting, even smoking, flames are easily realized at elevated pressures. In such flames, the effect of scattering and absorption by soot particles on the LII signal can no longer be neglected. Soot particles between the region of interest and the detector dissipate the pristine LII signal [44,215,216], whereas part of the light from incandescent particles along the laser heating but outside the region of interest is scattered towards the detector, contributing to the signal [214]. The extinction of LII signal can to some degree be remedied for an axisymmetric flame by inferring the pristine LII signal from the LII signal measured and the line-of-sight transmission measurements [209,214]. However, the fact that scattering is wavelength dependent brings more challenges to the system. Temperature pyrometry techniques, either two- or multi-colour, are biased in the presence of strong selective scattering. Scattering and absorption act on the laser light as well. Intensity of the

laser light may become variable along its path inside the flame, and laser-beam or -plane profile may become distorted due to the gradients of soot concentration in a flame [202].

Shrinking flame size accompanies increasing soot loading for a co-flow diffusion flame at elevated pressures. These changes co-act to increase temperature gradients within the flame. As a result, beam steering deviates the LII signal and the laser light from their ordinary track. This means that the true location of the measurement region can no longer be known, and in worst case, some light may even miss the optical elements and the detection sensor. Besides, the contraction in the volume of soot presence creates a need for refined laser probing and detection. In the extreme case, a reduction in LII signal was observed at high pressures because cross-sectional area of the laser had been decreased to resolve the shrinking flame, even though an increase in LII signal would had been expected from increasing soot concentrations [214]. In any case, measurements at high pressures benefit from the high spatial resolution of the LII technique.

The lack of the complete comprehension of the physical processes occurring following the laser heating and the dependence of these processes on pressure lead to uncertainties in the interpretation of the experimental data. Once again, the energy balance of the particles and competing heat transfer mechanisms are part of the ambiguity. At super-atmospheric pressures, heat conduction is not only the dominant mechanism but also in the extreme, it may become so fierce that the time scale of the possible duration of detection reduces to a point where the laser pulse and measurement time length can no longer be assumed instantaneous [208]. In one study [214], change in the decay rate of the LII signal with pressure was compared with predictions in the relevant modeling work [217]. Although the trends were matching, the agreement between the model and experiments was considerably weak. The increase in the decay of the LII signal due to increasing pressure was found to be considerably less in the experiments than what the model predicts. It was speculated [214] that the discrepancy can be explained by increasing primary particle sizes at elevated pressures. This explanation may not apply to all flame configurations since some studies [178,210] found that the trend between particle diameter and pressure is not always a definite one or one that is predicted. Nevertheless, a slight increase in primary particle size can result in large differences in the LII signal since laser induced incandescence is more sensitive to bigger particles.

Furthermore, models usually include the effect of the pressure in a superficial manner. Of the nine models reviewed in [202], only two incorporate all the possible regimes for conduction heat transfer, namely, free-molecular flow, transition, and continuum regimes. The effect of pressure is quite different in these regimes; a shift from free-molecular flow regime to continuum regime minimizes the effect of pressure on heat loss from soot [209]. However, it was observed that the decay rate of the LII signal still has a significant dependence on pressure in the transition regime [209].

Laser induced incandescence models often omit the effect of pressure on vaporization soot temperature and peak soot temperature. It was predicted that as pressure increases, vaporization starts at a higher temperature, and as a result, the need for excitation energy to attain vaporization temperatures increases [209]. Fortunately, these predictions did not materialize during the experiments [209]. It is also encouraging that the reduction in peak soot temperature due to higher heat transfer rates by conduction at elevated pressures was found to be substantially less [214] than what the model predicts [217]. These observations corroborate the view that LII signals at different pressures are comparable without significant bias.

Finally, the effect of pressure on LII calibration cannot be disregarded. In most implementations of laser induced incandescence theory, the practitioner measures a signal that is in strong correlation with soot volume fraction, but in arbitrary units; therefore, if absolute soot concentration is desired, the measured LII signal must be paired off with the results of a diagnostics system that is capable of providing absolute soot volume fraction. This calibration is usually done using the most basic flame configurations for simplicity and to improve the quality of the calibration. For the reasons discussed above, LII system is expected to read different LII signals for the same soot concentrations at different pressures. The inclusion of pressure effects in the analysis of the data cannot compensate for all the bias. It is not feasible to calibrate LII at all working pressures, but calibration pressure can be chosen as the middle pressure [44]. Yet again, results of the calibration systems are not impartial to pressure. For example, uncertainties in predicting refractive index of the soot at different pressures may result in substantial errors when using light extinction methods for calibration [209]. Another source of error is emissions from sources in a flame other than soot. This error more or less applies to all optical techniques that measure soot concentration. Although C_2 is anticipated to be a probable source of fluorescence and thereby a possible cause of intervention at high pressures [202], a noticeable emission from C_2 was not observed at elevated pressures [209,210].

An alternative would be using a realization of laser induced incandescence that does not need calibration. Such a system is explained in [218], which measures absolute soot volume fraction by employing the knowledge of the temperature field obtained by two-colour pyrometry and by pre-calibration of the measured LII signals for their absolute intensity. The shortcoming of this system is associated with the temperature measurements at different pressures. Effects of changes in soot morphology with varying pressure superpose with the bias described by wavelength dependency of scattering [214,216].

All in all, LII is a robust technique to measure soot volume fraction and particle size distribution. In actual experiments at elevated pressures, it performs much better than predicted by assumptions based on theoretical grounds. Soot volume fractions measured by LII at high pressures agree reasonably well with those measured by another technique [214], and likewise, soot size distribution measurements by LII and TEM are in good agreement up to 10 atm in rich premixed flames. However, there are unresolved issues for particle size measurements at higher pressures [210,219].

3. Experimental studies of soot formation at high pressures

The literature on high pressure combustion is voluminous, but it becomes limited when one looks for soot-related studies; in fact, it is meager on the effect of pressure on soot concentration in a laminar diffusion flame. Fortunately, there has been an interest in this subject by multiple research groups over the last decade. The accumulated knowledge since the discovery of soot deposition in explosion studies in 1920–30s is very much scattered among different experimental methods, burners, and measurement techniques. In this section, the aim is to discuss relevant experimental studies in a chronological order, albeit not strictly, and to point out well established observations as well as inconsistencies. Available data are classified into two categories according to how a comparison of soot concentration was presented in the original studies: (a) studies that present line-of-sight integrated values of soot volume fraction or in any other lumped way and (b) studies that present local values of soot volume fraction (that could be obtained through an inversion algorithm or by direct local measurements). The latter is the state of the art today, even though it is rather recent in soot-related studies of laminar diffusion flames at high pressures. The

dependency of soot concentration in a flame on ambient pressure can usually be expressed as a pressure scaling relationship in the form of a power law, i.e., $\propto P^n$, and this representation is frequently used in this section. The effect of pressure on soot morphology is not discussed in this section and deferred to Section 4.

3.1. Historical background

Early studies of explosion and flame spectra can be regarded as the forerunner of the systematic studies of soot formation at high pressures as often soot deposition was reported and quantified in these studies. Professor Bone of Imperial College and Dr. Townend published results from explosions of several mixtures in quite a few different explosion chambers in their 1927 book [220]. There had been the notion among the leading chemists of the 19th century that carbon is what is left when hydrogen is disentangled from hydrocarbon fuel (during the "preferential combustion" of hydrogen for fuel-rich mixtures). By 1927, this belief was mostly abandoned and criticized for its unconditional acceptance with no underpinning observation as such [220]: "it swayed men's minds during nearly the whole of last century [19th century], proving that dogmas are by no means the monopoly of theologians". Following research proved that a direct dissociation of the fuel into its elements is extremely unlikely. It was proposed instead that carbon formation involves a series of decomposition reactions followed by polymerisation and coalescence of decomposition products with simultaneously occurring dehydrogenation.

Methane–oxygen mixtures were mixed in a cylindrical bomb at a pre-explosion pressure of about 12.5 atm for equivalence ratios of 2, 3, and 4, and it was reported that 20% of the carbon in the fuel was converted into soot for the most fuel-rich mixture and none for others [220]. Ethane–oxygen mixtures with an equivalence ratio of 3.5 were studied at a pre-ignition pressure of slightly below atmospheric pressure, which reached to 1.5 atm following the ignition, in cylindrical and spherical chambers, and carbon conversion ratios of 7.6% and 18% were reported, respectively. The same rich ethane–oxygen mixture was detonated at an initial pressure of about 1.5 atm and was exploded at a pre-ignition pressure of about 25 atm, and in both cases, carbon conversion did not exceed 3.5%. Although no discussion was presented on why huge differences in carbon conversion was observed in seemingly identical conditions except for the chamber type and on why soot deposition was reduced as initial pressure was increased (as majority of the literature today suggests otherwise), it is not unreasonable to suspect that residence times played a major role in the differences observed; a comparison of flame duration was expressed in their remarks section, though no quantification was provided, and increasing soot deposition follows the same order as increasing flame duration. Another explanation was proposed in [221] that the different deposition characteristics observed in different chambers can be explained by different area to volume ratios of these chambers. As surface area increases per unit combustion volume, surface–combustion interactions become more important. Mixtures of ethylene–, propene–, trimethene–, and n- and iso-butene–oxygen with an equivalence ratio of 3 were exploded in a glass bulb for a pre-explosion pressure of between 0.5 atm and 1 atm, and curiously, no soot deposition was observed [220].

In the same laboratory, pre-explosion pressure of methane–oxygen mixtures was extended to 150 atm, and as a result, maximum pressures as high as 1500 atm were observed during the explosion [222]. The experiments for mixtures with equivalence ratios of 5, 4, 3, 2.66, and 2 showed that soot formation ceased at an equivalence ratio $\varphi = 2.66$ and below, down from soot conversion ratio of 26.3% at $\varphi = 5$ at a pre-explosion pressure of 6 atm. Once again, increasing pre-explosion pressures (thereby, maximum attainable explosion pressures) seemed to decrease soot formation. It was tentatively attributed to a possible effect of pressure on methane decomposition. It is unlikely that the effect of pressure is chemical, but most probably mechanistic or a combination of both. The length of time from the onset of explosion to reaching the maximum pressure was provided quantitatively; its increase is accompanied by an increase in soot deposition. An inverse correlation was observed for cooling rates and equivalence ratios, that is, richer mixtures showed lower rates of cooling. These two trends also appeared between various mixtures of slightly sooting methane–air and non-sooting methane–oxygen–argon. Methane–oxygen mixtures were also exploded for emission spectroscopy analysis, and a transition was observed to have taken place from banded spectrum to continuous spectrum as equivalence ratio is increased [223]. This is attributed to soot formation in these flames. Moreover, the spectroscopic analysis, when carried out for their continuous flames, showed a similar trend in the spectra with increasing pressure, but no soot deposition was observed.

Probably the first evidence suggesting that soot formation is enhanced at elevated pressures comes from a spectroscopic study of emission from flames. Smith [224] studied the effect of elevated pressures on pure ethylene and its various mixtures with hydrogen in a counterflow burner, which produces a flame that is believed [221] to be neither diffusional nor premixed but in between closer to a diffusion flame. Including even those of ethylene-lean, previously non-sooting flames started sooting after a composition-specific pressure was reached [224]. A specific pressure that leads to soot formation was also observed when the mixture of ethylene with various oxygen–nitrogen mixtures were exploded at sub- and super-atmospheric pressures. Oxygen replacement over nitrogen was found to reduce this critical pressure when ethylene fraction was kept constant. For comparison purposes, propane–air mixtures were also studied at sub-atmospheric pressures, but due to the fuel effects on sooting tendency, no soot formation was observed.

A remarkably comprehensive study of flame spectra [42] was published in 1956 that reports results from several possible diffusion and premixed flames of methane, ethylene, hydrogen, carbon monoxide, and methanol with air or oxygen. It is not easy to briefly summarize such extensive data, but in short, in the flames of most hydrocarbons (i.e., fuels excluding hydrogen and methanol), a continuous broadband radiation appeared as pressure was increased for flames that did not exhibit any at atmospheric pressure, and for those that did exhibit and those that acquired with an increase in pressure, the intensity of the emission increased with pressure. Even though there were some other contributors to the continuous radiation particularly in the flames of carbon monoxide and of hydrogen, the main contender was believed to be soot particles [42]. Discussing the effect of pressure on premixed flames, the authors [42] did not corroborate with Smith's [224] deduction that increasing pressure would ultimately lead even the leanest premixed flames to soot. Yet, they [42] concluded that for normally non-sooting diffusion flames of hydrocarbons, soot formation occurs eventually at a critical pressure. In some cases, soot yield increased so much that experiments had to cease, and in one particular case, an unexpected carbon formation was reported at the exit of the slot burner. The phenomenon what the authors [42] call "graphite formation" was reported in other studies at different periods of history with descriptions as "branching" growth of carbon with a look of "hard vitreous type" [41] and "soot accumulated around the fuel tube exit" [44]. This exotic crust-like solid carbon, usually clinging to the burner exit, is more recently documented in [43] with sequences of images showing the temporal evolution of the fuel into carbon.

3.2. Early studies with no measurements of local soot volume fraction

Parker and Wolfhard [41] studied sub-atmospheric co-flowing diffusion flames of acetylene with air and oxygen, and they observed that the rate of soot formation was adversely affected by reducing pressure, eventually to a point where soot formation no longer occurred. They were the first to observe that the volume occupied by soot particles inside a co-flow flame, distinguished by its distinctive colour, and the relative location of this volume inside the flame depend on pressure. Their findings [41] are complementary to those of Smith [224] that there may be a critical pressure for the flame of any fuel below which soot formation does not occur, or in a similar fashion but with a different implication, for the flame of any carbon-containing fuel that is known to be non-sooting at atmospheric pressure, there may be a high pressure that sooting occurs. They [41] also proposed that co-flow diffusion flame heights should be independent of pressure. This is explained by arguing that as pressure increases, the effect of increasing flow velocity is counterbalanced by the effect of poor mixing due to decreasing diffusion rates. This constant flame height prediction was partly validated by their observations that non-sooting flames complied with it, whereas sooting and smoking flames did not agree with constant flame height prediction. The convenience of pressure independence of the flame height is specific to the co-flow arrangement due to its symmetry, and the same assumption, later, is elegantly used by Roper [66,225] in the derivation of his famous theoretical and semi-empirical equations to predict the co-flow flame heights.

Schalla and co-workers [226,227] studied diffusion flames of several hydrocarbon fuels up to 20 atm. Two sets of experiments were conducted using similar experimental rigs except for the burners. The first burner, a wick lamp of controllable flow rate, allowed measurements up to 12 atm but mostly at and below 4 atm. This burner had the advantage that flames of liquid fuels could be easily stabilized and thus studied at elevated pressures. The flow rate was varied until the smoke point of the flame was reached, and the procedure was repeated at each pressure, i.e., 0.5–4 atm, for each fuel studied, e.g., pure hydrocarbons like octane isomers and blends like JP-4. Inversely proportional to pressure, smoke point flow rates of the fuels showed different degrees of sensitivity to pressure changes. Second, a tubular burner was used to study the flames of ethane and ethylene with the difference that smoke point flame height was reported for these flames instead of the flow rate. Flame heights were found to increase linearly with the inverse of the pressure for both fuels, but again showing different sensitivities. Fuel flow rate or the height of a flame at smoke point is a measure of the flame sooting tendency. Thus, their findings confirm the soot-enhancing feature of increasing pressure. They concluded that the effect of pressure must be specific to diffusion flames, where the rate of mixing is controlled by the pressure-dependent diffusion. This conclusion seems to be not true, though is an appealing argument; Fenimore et al. [228] showed that sooting tendency of a premixed flame is a function of pressure by showing that soot-point mixture strength is indeed affected by pressure, that is, the ratio of the fuel to oxidizer at the sooting limit decreased as pressure was increased for all the fuels studied. Further, Macfarlane et al. [229] studied soot formation from atmospheric pressure to 20 atm in laminar and turbulent premixed flames. They proposed a scaling factor of $P^{2.5\sim3.0}$ between the soot yield and pressure for flames of selected C_5 and C_6 hydrocarbons and air.

Milberg [39] measured the soot deposition rate on a glass wool filter connected to a pressure chamber for co-flow diffusion flames of acetylene and air at pressures from about 0.1 atm to 0.5 atm. Three burner geometries were used to study under-, ideal- (pseudo-stoichiometric—to be stoichiometric if premixed), and over-ventilated flames keeping the exit velocities of the co-flowing streams equal. He [39] proposed that smoking rate (soot formation − destruction) is not affected by the degree of ventilation and is linearly proportional to pressure increase. The volatile part of the soot was also analyzed for its structure, finding out the main constituents as small PAHs [39]. Similar fused-ring structures were observed when a similar analysis was performed on tars produced at 8 atm from benzene–air flames [229]. These can be regarded as early evidences for the PAH-based theory of soot formation.

A review of the literature on the effect of pressure on soot formation was published in 1972 [221]. Although most of the studies on soot formation at elevated pressures have been published after this date, this review serves as a good reference for anyone who desires a wider discussion of these early studies or who is interested in subjects omitted in this review such as droplet combustion at elevated pressures.

In their 1977 NASA report, Miller and Maahs [38] described the details of a newly developed experimental apparatus for high pressure combustion studies that can sustain stable diffusion flames up to 50 atm. The design of their co-flow burner and pressure chamber was innovative in many ways, and the experimental work has been seminal in understanding the effects of pressure on co-flow diffusion flames. Therefore, many of decisions made by the authors during the design phase have become the norm in the following studies such as that flames should soot, but not smoke, and condensation of water vapour should be controlled. A major drawback of co-flow diffusion flames related to high pressure combustion studies is that the limits of flow rates that generate a stable non-smoking flame shrink as pressure increases. For the lower limit, this is because higher reaction rates induced by increasing pressure reduce the thickness of the reaction zone, and a thinner reaction zone means that the reactant flow mechanism cannot as easily make up for the effect of the slightest disturbance in the reaction zone [38]. In designing this simple experimental set up, the major intention of the authors was to obtain data on nitric oxide formation that could be useful for understanding droplet combustion in gas turbines, yet a number of other measurements were made such as flame temperature, height, stability, and luminosity. Temperatures of soot particles were calculated by measuring soot emission at two wavelengths for methane–air diffusion flames within the pressure range of atmospheric pressure to 50 atm. Temperature measurements were then used to calculate carbon concentration in these flames. Flame shape was found to change from a voluminous outwardly curving (convex) appearance to a slim inwardly curving (concave) appearance; the change in flame shape was most prominent at lower pressures and got weaker above 20 atm. The contraction of the flame with increasing pressure was attributed to the emergence of soot particles and the subsequent increase in their volume fraction, that is, massive compared with gaseous species, soot particles are not willing to spread out radially, and when they exist in high concentrations, they dictate the flame shape [38]. Flame height was found to vary slightly with pressure especially between 30 atm and 50 atm, which is contradictory to what was predicted earlier by [67,230] and later by [66]. For a possible reason of this discrepancy, the authors [38] pointed out the existence of soot particles in their flames. The soot concentration increased by three fold from 2.5 atm to 20 atm. But as the pressures reached to 40 atm (and above), the change in soot concentration almost leveled off. It was not only the soot concentration changing, but also the region in which soot particles reside changed in appearance. This region, originally around the flame tip, extended down the flame as pressure was increased, and eventually made up most of the flame volume.

Increases in the concentration and coverage of soot led to an increase in light emission intensity. Consequently, increasing radiative heat loss marked a decrease in the maximum temperature.

Flower and Bowman did a number of experiments on the effects of pressure on soot formation. In the first set of experiments, they studied ethylene–air flames using a Wolfhard-Parker slot burner at pressures between 1 atm and 2.5 atm [231,232]. Extinction of laser light passing parallel to the longer side of the burner was measured in order to calculate soot volume fraction, and measurements were repeated along the direction parallel to the shorter side at selected heights. Total volume of soot over a plane perpendicular to the flow direction was inferred from integrating soot volume fraction values. They reported a scaling factor of $P^{1.7\pm0.3}$ for maximum soot volume fraction and integrated soot volume fraction. Particle size and number density were also calculated from scattering measurements and were found to increase with pressure. Thermocouple measurements of the temperature field showed about a 100 K reduction in the maximum temperature as pressure was increased from atmospheric pressure to 2 atm. These observations led the authors to conclude that increasing soot volume fraction is a collaborative result of increasing rates of surface growth and particle nucleation. However, care should be taken when adopting these results and comparing them with those in the literature because mass flow rates were varied linearly with pressure in order to keep measurements comparable at constant heights at different pressures. In a follow-up study, velocity measurements were made for the same configuration at 1 atm and 2 atm [233]. Peak axial velocities at selected heights were equal at different pressures, proving that residence times can be made independent of pressure in this burner type by keeping the burner exit velocity equal at all pressures. This makes results from same heights above the burner comparable at all pressures, notwithstanding that axial velocity increases with axial location due to buoyancy. On the other hand, pressure had an effect on transverse velocities, that is, the degree of air entrainment at different pressures were different. Recent modeling work shows that the effect of pressure via modifying air entrainment is indeed very significant suggesting that the effect of pressure can be regarded as being of a mechanical nature [58]. These velocity measurements when interpreted in the light of previously reported soot measurements by the same group suggest that the increase in soot yield previously observed is due to increased local rates of soot formation [233].

In the second set of experiments, the authors switched to a co-flow diffusion burner in order to achieve measurements at higher pressures, where the Wolfhard-Parker burner proved to be unsuitable due to its stability characteristics. Extinction measurements were performed along the centreline of ethylene–air flames at pressures between atmospheric pressure and 10 atm [53]. A scaling factor of $P^{1.2\pm0.1}$ was found for line-of-sight integrated soot volume fraction measurements. Working with an axisymmetric burner allowed to keep mass flow rates equal at different pressures without losing tractability of the results at selected heights from flames at different pressures. Therefore, increased soot volume fractions indicate a similar increase in soot yield. In fact, it was found that half of the carbon in the fuel is converted into soot at 10 atm. An extrapolation of the initial rate of increase in soot yield suggested that carbon in the fuel would appear only as soot at 18 atm.

Line-of-sight averaged soot particle temperatures were also measured for the same configuration for pressures between atmospheric pressure and 7 atm [54]. These temperature measurements [54], when compared with gas temperature measurements for a similar flame configuration (Ref. 14 in [54]), show that both particle and gas temperatures are in good agreement, and both decrease by increasing pressure. It should be noted that the flames studied in [53,54] were smoking flames, except for those at atmospheric pressure. Smoking flames and their suitability will be further discussed in Section 3.3.

Law et al. [48] studied inert diluted ethylene–air flames in a counterflow burner at pressures between 1 atm and 2.5 atm. Temperature effects were uncoupled from those of pressure and were eliminated by keeping the temperature constant at all pressures, which was accomplished by adjusting the nitrogen fraction in the fuel stream and replacing the same molar amount of nitrogen in the oxidizer stream by argon. A method for measuring sooting tendency in counterflow flames, which uses a similar reasoning to that of measuring smoke point flame height/flow rate in co-flow flames, is measuring soot-extinction strain rate. Measurements of the strain rate at soot-extinction show that a higher strain rate is necessary to suppress soot formation at higher pressures [48]. The authors suggested that the overall rate of soot forming reactions increases linearly with increasing pressure within the experimental pressure range they used.

Based on a postulate that the soot volume fraction that penetrates the laminar diffusion flame to cause the smoke height is controlled by the distance between the isotherms that specify the incipient soot formation and stoichiometric flame temperatures, Glassman [234] proposed that soot volume fraction scales with pressure as $P^{1.31}$. Flames under microgravity conditions were also analyzed, and it was predicted that pressure dependency is stronger in microgravity, i.e., according to P^2. The same postulate predicts the flame cross-sectional area to scale with pressure as $P^{-0.5}$. It is discussed in Section Section 1.1 that residence times in a co-flow flame are independent of pressure for an area pressure dependence according to P^{-1}. This is indeed what was observed numerous times by experimentation (e.g., [44,46,63]).

3.3. Smoke point fuel flow rate at high pressures

The smoke point test method [235] is claimed to be quantitatively related to the potential radiant heat transfer from the combustion products of the fuel, and it provides an indication of the relative smoke producing properties of kerosene and aviation turbine fuels in a diffusion flame. It is defined as the luminous flame height immediately prior to the flame emitting smoke. The measurement involves varying the fuel flow rate in a standard wick burner until the point at which the soot breaks from the tip of the laminar flame.

The smoke point [235], the maximum flame height beyond which soot just escapes from an axisymmetric laminar diffusion flame tip generated by a standard wick burner (or the maximum fuel mass burning rate without generating a smoking flame), has been used since 1940s to predict the sooting propensity of kerosene and gas turbine fuels. The smoke point is strongly dependent on the molecular structure of the hydrocarbon fuel [235,–240], and the maximum soot concentration in diffusion flames can be qualitatively related to the smoke point fuel flow rate [241]. Further it is shown that a linear relationship exists between smoke point values and the smoke point heat release rates [242].

Since the gas turbines operate at super-atmospheric pressures, there has been always a question mark whether an atmospheric laminar diffusion flame height would provide any indication of the amount of exhaust smoke of the gas turbine engine. Schalla et al. [226,227] conducted experiments with several fuels to measure the smoke points and the corresponding smoke point fuel flow rates as a function of pressure. They showed that the smoke point height decreases as the pressure is increased for all the fuels they considered. Their data for methane, ethylene and, ethane are

plotted in Fig. 3. Also shown in Fig. 3 is the findings reported more recently by Berry and Roberts [57] for ethylene and methane, which follow the same trend as the results reported in [227].

Schalla and McDonald [226,227] found that the reciprocal of the smoke point fuel mass flow rate scales with pressure approximately as $P^{1.0\pm0.2}$ for a range of fuels at pressures up to 12 atm. A selection of data from Schalla and McDonald are shown in Fig. 4 for liquid fuels. More recently Flower and Bowman [53] showed that for ethylene flames at various pressures the scaling of the smoke point fuel mass flow rate, $\dot{m}_{sp}$, is

$$\frac{1}{\dot{m}_{sp}} \propto P^{1.3} \tag{11}$$

in good agreement with the results of Schalla and McDonald [227]. However, Berry and Roberts [57]reported a completely opposite trend in the dependence of the smoke point fuel mass flow rate on pressure:

$$\dot{m}_{sp} \propto \exp[aP] \tag{12}$$

where a is about 0.19 for ethylene and 0.1 for methane. Data for ethylene and methane from [57] are shown in Fig. 4 in comparison with the data of Schalla and McDonalds [227]. The significant discrepancy between the two sets of results is puzzling. The only implication is that the experiments in [57] were such that fuel and co-flow air velocities were matched to avoid possible influence of velocity ratio of air to fuel on smoke point. However, it was shown by Lin and Faeth [243] that air/fuel velocity ratio is important only in nonbuoyant conditions (such as at sub-atmospheric pressures and at low gravity), and at atmospheric and above pressures the effect is negligible due to the dominance of strong buoyancy.

One of the critical parameters that should be kept constant is the fuel mass flow rate at high pressure soot experiments to have tractable measurements. The fuel mass flow rate that would be under the smoke point height at relatively low pressures may reach the smoke point condition at a higher pressure. The highest planned pressure should determine the fuel mass flow rate; otherwise, some of the flames would be smoking flames, which would complicate the analysis of soot formation and oxidation where residence times and temperatures would be difficult to define and measure. Luminous flame heights, under strongly smoking conditions, will not have the usual meanings, and proportionality to the

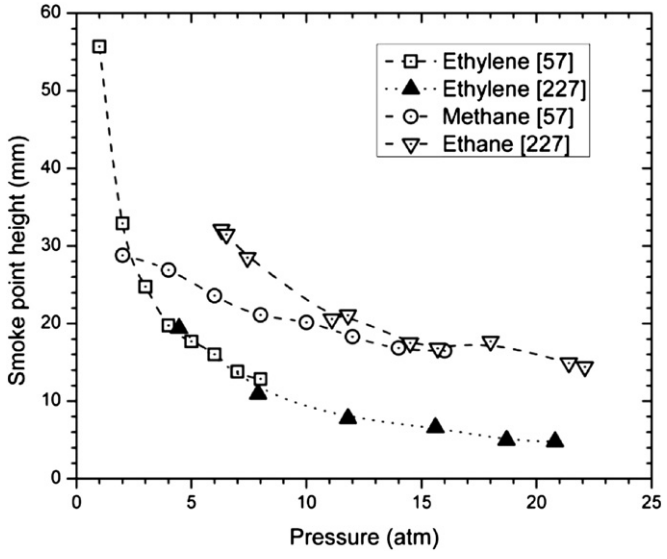

Fig. 3. Dependence of smoke point flame height on pressure for co-flow laminar diffusion flames. Data in this plot were taken from [57,227].

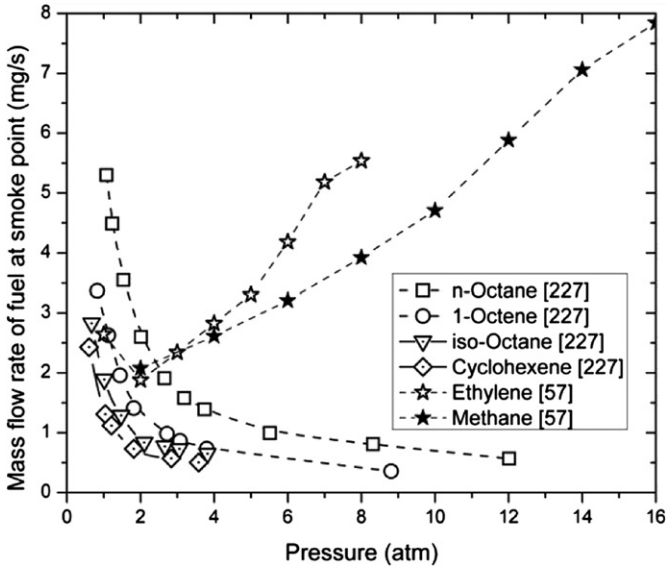

Fig. 4. Dependence of mass flow rate of fuel at smoke point on pressure for co-flow laminar diffusion flames. Data in this plot were taken from [57,227].

flame residence times may be lost. This behavior can be observed in the experimental flame height measurements reported in [244] as a function of pressure. Visible flame heights of propane, methane, and ethylene increase mildly from atmospheric to a few atmospheres and then start decreasing steeply with increasing pressure [244], Fig. 5. The turning pressures should correspond approximately to the smoke point fuel mass flow rates of these fuels. (Note that there is a typo in Table 1 of Ref. [244] where the unit of the mass flow rate should be mg/s, not g/s). On the same plot, Fig. 5, the visible flame height data from the senior author's laboratory are shown for several fuels. It is apparent that, as long as the fuel mass flow rate is under the smoke point mass flow rate, the visible flame height stays almost constant after about 5–10 atm.

Another point regarding the flame heights of the work reported in [244] is that, the heights shown in Fig. 5 for ethylene at atmospheric pressure cannot be replicated by using the Roper's correlation for circular burners [66]. Roper's correlation yields a flame height of about 33 mm for the given fuel flow rate whereas Fig. 5 indicates a flame height of 19 mm.

3.4. Recent studies with measurements of local soot volume fraction

Lee and Na [55] measured soot concentrations and temperatures in co-flow diffusion flames of air as oxidizer and pure ethylene and its various binary mixtures with air and propane as fuels. The experiments were carried out between atmospheric pressure and 4 atm, and two-colour pyrometry was used to measure temperature and to infer soot volume fraction. Line-of-sight averaged temperature measurements for the flames of pure ethylene show similar trends to those reported in [54] except for the middle region of the flame, where temperatures at different pressures did not come close to each other in this study. Flames of pure ethylene were smoking at above atmospheric pressure, similar to ones in [54], and they reported [55] the same low-temperature limit for soot oxidation, that is, 1400 K. Above atmospheric pressure, mixtures of ethylene and air and of ethylene and propane, as fuels burnt with air, showed synergistic effects in soot formation, that is, the resultant soot formation rate of the fuel mixture is higher than those of the individual fuels and the sum of the respective rates of the mixture components. They also [55]

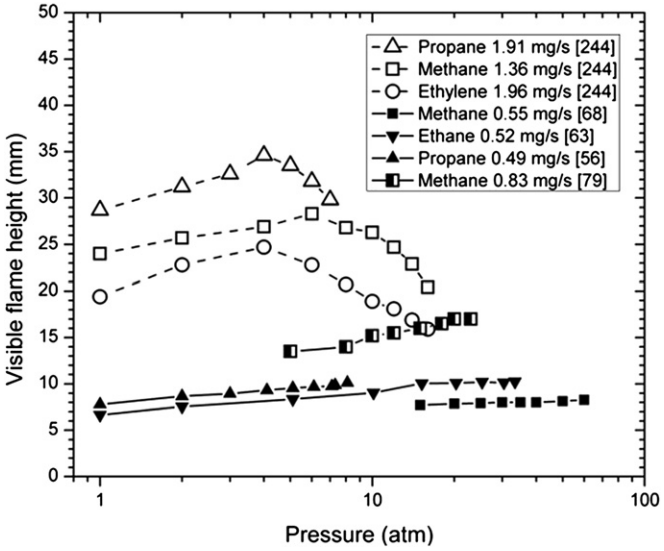

Fig. 5. A comparison of visible flame heights of smoking and non-smoking laminar diffusion flames as a function of pressure. Data shown by blank symbols are from [244], and around 4–5 atm they switch to becoming smoking flames. Non-smoking diffusion flame data are from [56,63,68,79].

provided the first radially resolved results of soot volume fraction at high pressures, albeit limited to one height only, by applying the Abel inversion to the line-of-sight measurements [55]. Based on the line-of-sight integrated and radially resolved soot volume fraction plots, scaling factors of $P^{1.26}$ and P^2 can be derived for the maximum soot volume fraction between 2 atm and 4 atm and for line-of-sight integrated soot volume fraction between 1 atm and 4 atm, respectively.

McCrain and Roberts [44] measured soot volume fraction for co-flow diffusion flames of methane–air and ethylene–air at pressures up to 25 atm and 16 atm, respectively. Light extinction technique was used to measure line-of-sight integrated soot volume fraction, and this in turn was used to calibrate the LII system. The distance between the radial peaks of soot, d, at slightly above the middle flame height was measured to vary with pressure as $d \propto P^{\sim 0.5}$ for both fuels. An inverse square root scaling between diameter and pressure leads to an inverse relation between area and pressure; this proves experimentally that residence times are independent of pressure for axisymmetric burners. Line-of-sight integrated soot volume fraction scaled with pressure as $P^{1.0}$ at 65% of the flame height and as $P^{0.6}$ at 85% of the flame height for pressures up to 10 atm, and peak soot volume fraction scaled as $P^{1.2}$ over a pressure range of 2–25 atm for methane–air flames. And for ethylene–air flames, line-of-sight integrated soot volume fraction scaled with pressure as $P^{1.2}$ at 85% of the flame height for pressures up to 10 atm, and peak soot volume fraction scaled as $P^{1.7}$ over a pressure range of 1–16 atm. This means that soot formation in ethylene flames is more sensitive to changes in the ambient pressure than in methane flames. Also corroborates this is that the slopes of the relationships of pressure with smoke-limit flame height and with volumetric fuel flow rate are steeper for ethylene flames than those for methane flames [57]. Soot particle temperatures were measured for the flames of ethylene and air over a pressure range of 1–8 atm by using two-colour pyrometry technique, and it was found that peak temperatures of flames at smoke point reduced as much as 250 K, whereas the decrease in temperature was almost 400 K when the mass flow rate was kept constant [59].

Darabkhani and Zhang [245,246] studied co-flow diffusion flames of methane and air at elevated pressures in order to reveal

Table 1
Summary of experimental results on the pressure dependence of soot in laminar diffusion flames.

Refs.	Pressure range [atm]	Fuel and fuel flow rate [mg/s]	Pressure scaling factor n in [soot] $\propto P^n$		
			Path integrated maximum soot	Local maximum soot	Maximum conversion of carbon into soot
[53]	1–10	Ethylene 1.9, 2.7, and 4.4	1.2 ± 0.1		
[55]	1–4	Ethylene 3.4	1.26	2 (20 mm above burner rim)	
[44]	1–16	Ethylene 1.13	1.2	1.7	
[44]	1–25	Methane 1.1	1	1.2	
[46]	5–20	Methane 0.55	1.3	2	1
[46]	20–40	Methane 0.55	0.9	1.2	0.1
[56]	1–2	Propane 0.49	3.4		3.3
[56]	2–7.3	Propane 0.49	1.4	1.8	1.1
[40]	30–60	Methane 0.55			0.33
[60,68]	10–40	Methane with pure oxygen 1.1	1.7	1.5	1.2
[60,68]	50–70	Methane with pure oxygen 1.1		−2.3	−3.8
[60,68]	70–90	Methane with pure oxygen 1.1	−10	−7.6	−12
[63,239]	2–5	Ethane 0.52	2.3	2.4	2.2
[63,239]	5–15	Ethane 0.52	1.4	2.4	1.1
[63,239]	15–33	Ethane 0.52	1	1.1	0.4
[64,68]	10–30	Diluted ethylene 0.27	1.62	1.76	1.36
[79]	5–10	Methane 0.83	1.12	2.2	0.92
[79]	10–20	Methane 0.83	1.12	0.6	0.68
[79]	2–10	Ethane 0.78	1.61	2.24	1.33
[79]	10–15	Ethane 0.78	1.08	1.52	0.58

the effect of pressure on flame stability. They reported that pressure is effective on the amplitude of the flame oscillations as well as oscillation frequency. The effect of increasing pressure is attributed to the increase in the size of toroidal vortices surrounding the flame jet, which interferes with the flame. Visualization of methane–air co-flow diffusion flames at 1, 6, and 12 atm shows indeed that the layered concentric flow at atmospheric pressure is replaced by an intricate surrounding with many recirculation zones as pressure is increased, and disorder draws near the flame front at 12 atm [191]. It is thought [247] that when mass flow rate is kept constant in co-flow experiments, the ratio of buoyancy forces to inertial forces varies with varying pressure. Flames become less stable with increasing pressure as gravitational acceleration becomes more pronounced. However, the overall effect of pressure on flame stability cannot be a purely aerodynamic one; increasing soot concentration in a flame also influences the flame structure and dynamics. This effect is usually towards stabilizing the flame by enhancing heat transfer towards the burner and by streamlining the flow. In a similar but more-extensive work from the same

laboratory, flame structure and stability were studied for flames of ethylene–, methane–, and propane–air at up to 16 atm [244]. Flame heights were found to vary with pressure, having their peak at a pressure specific to the fuel type. As expected from this observation, the cross-sectional area of the flames did not follow the theoretical prescription, i.e., $A \propto P^{-1}$. The scaling factor was found to be -0.8 ± 0.2 for ethylene, -0.5 ± 0.1 for methane, and -0.6 ± 0.1 for propane flames. The disparity with other studies is related to the scaling effects of the burners and to different flow rates used in different studies. Although not explicitly stated, it is apparent from the pictures of the flames that soot breakthrough is present in some of the flames studied, as discussed in detail in Section 3.3. Expectation of a constant flame height is not realistic for a pressure range in which buoyancy-controlled flames are replaced with flames whose structure is partially controlled by smoke escape from the tip of the flame envelope. The same caution should be observed in comparing other parameters between studies that involve smoking flames (e.g., [44,53–55]) and those that does not (e.g., [40,46,56,63]. The effect of soot liberation can also be seen in measurements of the temperature field of ethylene flames from atmospheric pressure to 10 atm [248]. While the maximum soot temperature decreased by 200 K, the minimum soot temperature decreased by 700 K due to the cooling effect of smoking.

The collaboration between the University of Toronto, and the National Research Council of Canada resulted in the development of a new pressure chamber design (see Fig. 6). The chamber has an internal height of 0.6 m and an internal diameter of 0.24 m, large enough to accommodate multiple burner types, and it has a maximum design pressure of 110 atm. The chamber allows optical access at 0, 90, and 180° through view ports housing quartz windows. Thus, line-of-sight and scattering measurements can be done simultaneously. The key components of the experimental set up (excluding LOSA) are shown in Fig. 7. This chamber design and a new co-flow burner design led to the first detailed data sets of radially resolved soot concentration and soot temperature at elevated pressures [46]. Following studies, which share the same design for the chamber and the burner, have chosen fuel mass flow rates, where feasible, such that the carbon mass flow rate matched that in the pioneering study. This lineage—all of the studies summarized below in this section—provided an extensive database, one that can be compared quantitatively, on the effect of pressure on soot formation for various fuels. Thomson et al. [46] employed SSE and LOSA techniques to measure soot volume fraction and temperature for co-flow diffusion flames of methane–air at pressures between 5 atm and 40 atm. Results obtained from both techniques agreed well, within 30%. There may be several reasons for small discrepancies that add up. For example, it was argued that light extinction techniques are expected to bias towards higher soot concentrations because the light extinction measured is ascribed to absorbtion only in the calculation, where in fact, Rayleigh approximation does not always hold valid that scattering becomes nonnegligible. It was shown later that LOSA when corrected for scattering agrees well with absolute-intensity calibrated LII technique in measuring soot volume fraction measurements at elevated pressures [214].

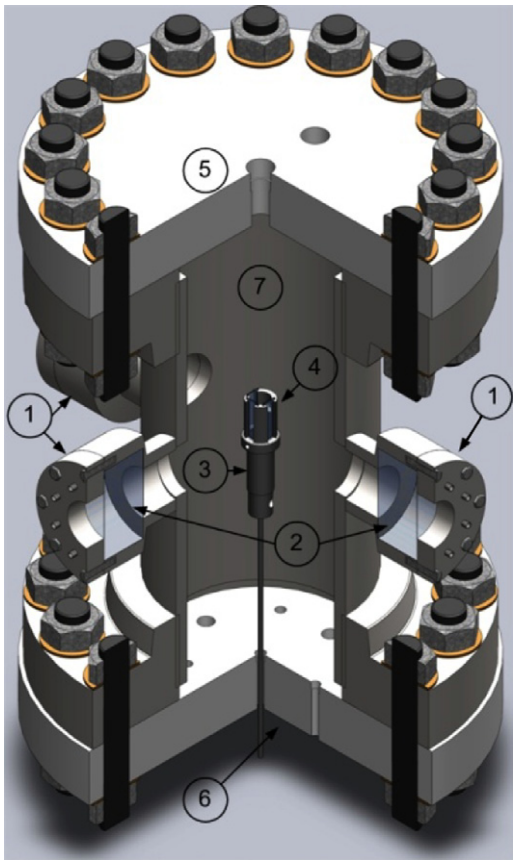

Fig. 6. A cutaway view of the high pressure chamber at UTIAS, University of Toronto: (1) Optical access ports; (2) Quartz windows; (3) Burner assembly (4) Chimney assembly; (5) Upper flange housing the exhaust, safety valves, and pressure transducer; (6) Lower flange housing air, fuel pipes and wiring; (7) Combustion chamber.

Flame shapes were examined up to 80 atm, and similar trends to those observed in [38] were evident [46]. Flame heights changed slightly with pressure between atmospheric pressure and 40 atm, but cross-sectional area of the flames followed the theoretical prediction with an uncertainty of ±0.1 for the power factor. Power law relationship between soot concentration and pressure existed in two distinct regimes. Maximum soot concentration scaled with pressure as P^2 and $P^{1.2}$ for pressures between 5 atm and 20 atm and between 20 atm and 40 atm, respectively. Maximum soot volume fraction does not directly correlate with sooting tendency because an inevitable result of the shrinking flame diameter is an increase in local soot volume concentrations even if the soot yield is constant.

A better measure of sooting propensity is the carbon conversion, which is the percentage of fuel's carbon content converted to soot. Peak carbon conversion scaled with pressure as P^1 and $P^{0.1}$ for pressures between 5 atm and 20 atm and between 20 atm and 40 atm, respectively. Maximum conversion increased from 2% at 5 atm to 9% at 40 atm. This shows that increasing pressure, apart from increasing local soot concentration due to its effect on flame shape, increases soot volume fraction through enhancing the soot formation mechanism. However, the reduction in the rate of the increase in peak conversion with pressure is indicative of diminishing precursors of soot. In order to maintain backwards compatibility in comparing the results in this study with the previous results in the literature, line-of-sight integrated soot volume fractions were calculated. Once again, two distinct regimes were recognized for the maximum line-of-sight integrated soot volume fraction, that is, it scales with pressure as $P^{1.3}$ and $P^{0.9}$ for pressures between 5 atm and 20 atm and between 20 atm and 40 atm, respectively. It was also noted that soot inception occurs closer to the burner exit as pressure was increased.

Temperature measurements reveal that this is due to heat transfer to the region of fuel decomposition increasing with pressure. Increasing soot loading in the flames resulted in an increase in radiative heat loss. This led to lower flame temperatures. Conversely, temperature gradients were increased as a result of increasing gradients of soot concentration. Radial temperature

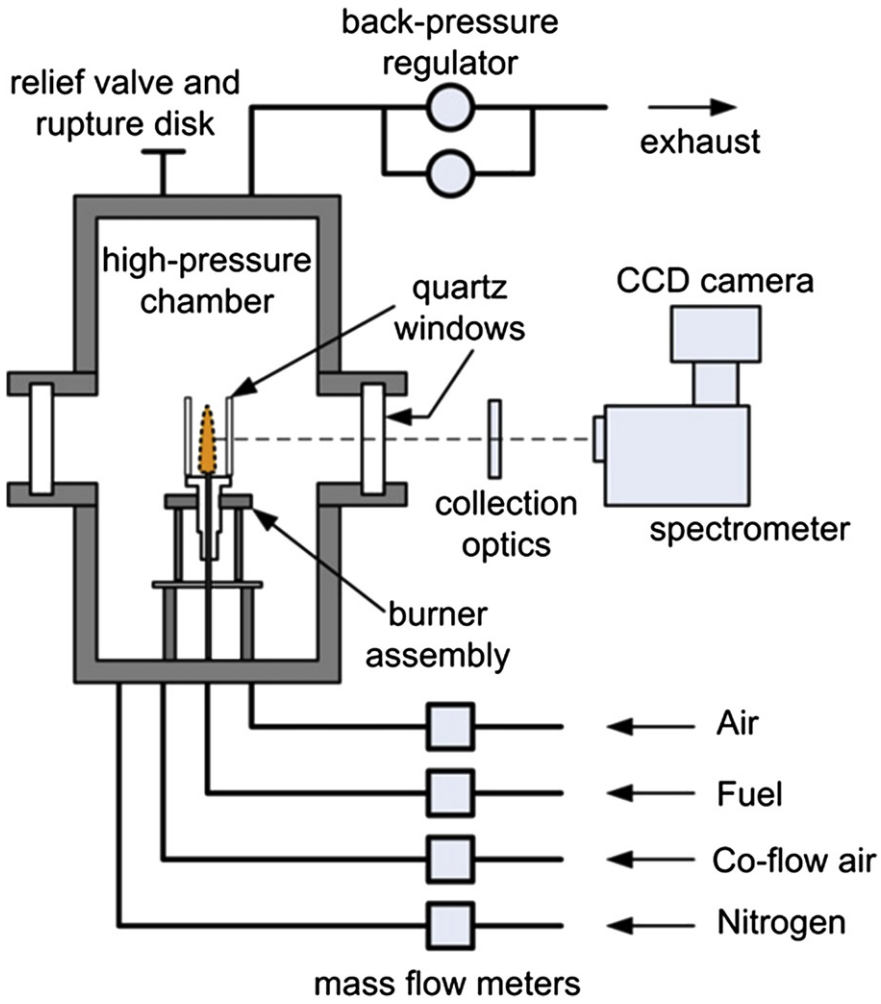

Fig. 7. A schematic of the high pressure combustion experimental layout, at UTIAS, University of Toronto [65].

gradients reached to 1000 K/mm at 40 atm at the height where the peak radial temperature gradient was observed as 400 K/mm at 5 atm. Overall in the flame, the peak radial temperature gradient was observed as 1300 K/mm.

Line-of-sight averaged temperatures show that the reduction in temperature with increasing pressure was smaller in the upper portion of the flame in contradiction to the results in [54]. Flames, as being non-smoking in this study [46], present a soot-oxidation region in the upper half. It is therefore expected for these flames that temperature drop due to enhanced radiative heat loss at elevated pressures would be partially made up for in the upper portion of the flame by the increased amount of heat that becomes available from the oxidation of greater amount of soot.

Joo and Gülder [40] continued studying methane–air flames in the same flame arrangement and did measurements at pressures up to 60 atm. Measurements at pressures exceeding 60 atm was not possible in this experimental configuration because the fuel persistently transformed into a liquid substance, speculatively with the help of the entraining water vapour into the fuel upstream [61]. As seen in Fig. 8a, maximum soot volume fraction increases from 14 ppm at 10 atm to 180 ppm at 60 atm. The results [40] were consistent with those in [46] except that peak carbon conversion scaled with pressure as $P^{0.33}$ between 30 atm and 60 atm as compared to a scaling factor of 0.1 reported in [46]. It was argued that the pressure sensitivity of soot formation in this study did not decrease as much because flame heights were found to be constant between 10 atm and 100 atm as opposed to a reduction in flame height above 20 atm observed in [46]. The authors [40] attributed this to a likelihood of an error being made in the calibration of the fuel flow rate in [46]. The maximum carbon conversion to soot was 12.6% at 60 atm. The cross-sectional area of the flame exhibited the inverse proportionality to pressure. Higher soot concentrations and the contraction of the flame led to greater rates of soot transport and higher radial gradients of temperature, as much as 1600 K/mm. Temperature drop with increasing pressure was explained by that less energy was generated in the first place due to incomplete combustion, and more heat was lost by radiation to the environment and by conduction to the flame core.

Joo and Gülder [60] also studied methane–oxygen flames at pressures up to 100 atm. In this study, fuel mass flow rate was chosen twice the methane flow rate in [40,46]. The methane flame gave a completely new appearance when burnt with pure oxygen. There appeared an inner flame, which was soot-laden and similar to the flame type expected from hydrocarbon–air flames, and a blue outer flame, which looked bulbous at atmospheric pressure. To explain the transformation in flame appearance, species concentration and temperature were evaluated using an axisymmetric flame code [249,250] employing GRI-Mech 3.0 reaction mechanism [251]. It was proposed that hydrogen, having a greater diffusivity, can penetrate into the oxygen stream more-easily than

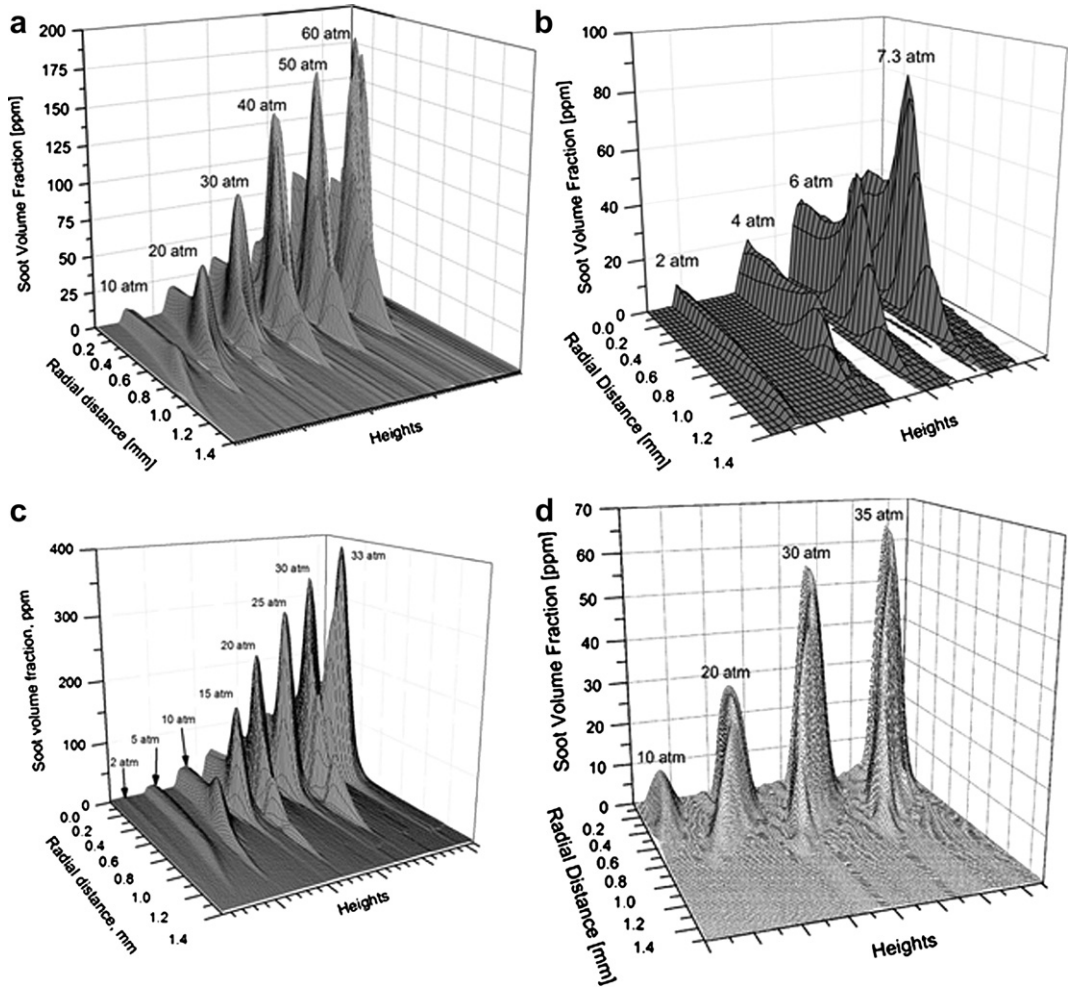

Fig. 8. Three-dimensional renditions of the soot volume fraction as a function of pressure and the spatial location within the flame for co-flow laminar diffusion flames. It should be noted that the "Heights" axis is a repeating coordinate representing successive height measurement locations from the burner tip for each pressure. m_c corresponds to the mass flow rate of carbon in the fuel. Measurements were performed using the spectral soot emission technique. (a) Methane–air flames, $m_c = 0.41$ mg/s [40]. (b) Propane–air flames, $m_c = 0.40$ mg/s [56]. (c) Ethane–air flames, $m_c = 0.41$ mg/s [63]. (d) Ethylene (nitrogen-diluted) – air flames, $m_c = 0.23$ mg/s [64].

other decomposition products of the fuel. As a result, a "stratified flame" could be created. This flame has a structure which transforms from a diffusion flame at its boundary with the inner flame to an increasingly premixed flame towards the outwards. The change in the flame shape with pressure was not radically different from that observed in hydrocarbon–air flames. Coexisting flames got slimmer with increasing pressure, the outer flame at a higher rate than the inner flame, and both flames curved inwards. Flame heights of the inner flame and the blue flame significantly decreased with pressure. The decrease in the blue flame was continuous over the pressure range but the inner flame reached a constant height at 50 atm.

According to the authors [60], flame heights did not stay constant, in contradiction to the theoretical prediction, because of a possible deviation in the pressure dependency of molecular diffusion from $D \propto 1/P$ and because of the greater magnitude of temperatures observed in pure oxygen flames. Surprisingly, the cross-sectional area of the inner flame showed inverse proportionality to pressure between 10 atm and 40 atm, the pressure range where the reduction in the flame height was observed, and showed a progressively increasing reduction above 40 atm, where the flame height was constant.

The cross-sectional area of the outer flame was in agreement with the inverse proportionality over all pressures. Soot volume fraction and temperature measurements were performed using the SSE technique. Among the soot volume fraction profiles reported by using the same burner, that of methane–oxygen flames have shown the least resemblance to one that could be characterized by a succession of power laws. Nevertheless, three regimes can be inferred. Maximum line-of-sight integrated soot volume fraction scaled with pressure as $P^{1.7}$ and P^{-10} for pressures between 10 atm and 40 atm and between 70 atm and 90 atm, respectively, and showed an irregular profile between 40 atm and 70 atm [68]. Maximum soot volume fraction scaled as $P^{1.5}$ for pressures between 10 atm and 40 atm, $P^{-2.3}$ between 50 atm and 70 atm, and $P^{-7.6}$ between 70 atm and 90 atm [60]. Increasing the pressure, maximum soot volume fraction started from 7 ppm at 10 atm, peaked as 55 ppm at 40 atm, and reduced down to 4 ppm at 90 atm. Peak carbon conversion scaled with pressure as $P^{1.2}$ for pressures between 10 atm and 40 atm, $P^{-3.8}$ between 50 atm and 70 atm, and P^{-12} between 70 atm and 90 atm. Maximum conversion did not exceed 2% at any pressure. The reversal in the carbon conversion trend after 40 atm suggests that the change in the sensitivity of carbon conversion to pressure cannot be explained only by a reduction in the concentration of precursors. Instead, there may be some chemical effects of pressure that take over mechanistic effects at a critical pressure. Temperature measurements corresponded to a limited region of the overall flame because soot

particles were only present in the inner flame. In general, temperatures were much higher than those observed in hydrocarbon–air flames, and the maximum radial temperature gradient was as high as 4000 K/mm.

Bento et al. [56] studied propane–air flames between atmospheric pressure and 7.3 atm using SSE and LOSA. Results from SSE and LOSA agreed within 30%, in agreement with the results of [46]. Flame heights were measured and found to be constant within 10%, and the flame cross-sectional area exhibited inverse proportionality to pressure. Maximum line-of-sight integrated soot volume fraction and peak carbon conversion were found to scale with pressure as $P^{3.4}$ and $P^{3.3}$, respectively, for pressures between 1 atm and 2 atm and $P^{1.4}$ and $P^{1.1}$, respectively, for pressures between 2 atm and 7.3 atm. Maximum soot volume fraction increased from trace amounts at atmospheric pressure to about 85 ppm at 7.3 atm, showing a scaling factor of 1.8 between 2 atm and 7.3 atm (see Fig. 8b). At the highest pressure, one fifth of the carbon in the fuel was converted into soot. Temperature measurements showed trends similar to those in [40,46]. The highest radial temperature gradient was reported as 1000 K/mm and was observed at the highest pressure studied. Line-of-sight averaged centreline temperatures at the lower half of the flame (soot formation region) resembled those in [54].

Mandatori and Gülder [63] studied ethane–air flames between atmospheric pressure and 33 atm using SSE. Flame heights were found to be constant within the pressure range of 10–33 atm, but to increase from atmospheric pressure to 10 atm. As seen in Fig. 9, however, the flame cross-sectional areas calculated from radial peaks of soot volume fraction and temperature showed inverse proportionality to pressure within the pressure range of 2–33 atm. Fig. 10 shows soot volume fraction and soot temperature profiles in a single plot. The peak temperature is located at a greater distance to the flame centreline, but the distance between the peaks of temperature and soot volume fraction decreases as pressure increases (see Fig. 11). The power law was not definitive along the whole pressure range but three distinct regimes may be inferred. Maximum line-of-sight integrated soot volume fraction scaled with pressure as $P^{2.3}$ for pressures between 2 atm and 5 atm, $P^{1.4}$ between 5 atm and 15 atm, and P^{1} between 15 atm and 33 atm.

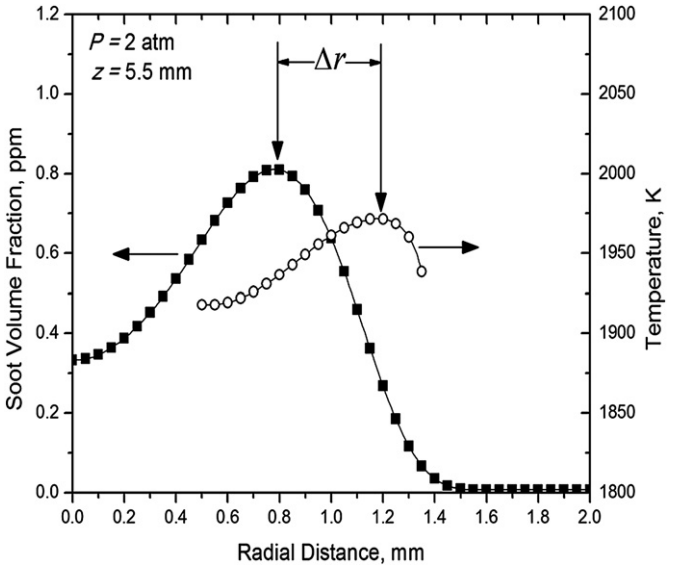

Fig. 10. Relative positions of the temperature and soot volume fraction profiles at 2 atm at a flame height of 5 mm for ethane–air co-flow laminar diffusion flames. Mass flow rate for carbon in the fuel, $m_c = 0.41$ mg/s. Mass flow rate of ethane, $m_f = 0.52$ mg/s. Measurements were performed using the spectral soot emission technique [63].

Maximum soot volume fraction scaled as $P^{2.4}$ and $P^{1.1}$ for pressure ranges of 2–15 atm and of 15–33 atm, respectively [252]. As seen in Fig. 8c, maximum soot volume fraction increases from less than 25 ppm at 5 atm to around 375 ppm at 33 atm. Peak carbon conversion scaled with pressure as $P^{2.2}$ for pressures between 2 atm and 5 atm, $P^{1.1}$ between 5 atm and 15 atm, and $P^{0.4}$ between 15 atm and 33 atm [63]. At 33 atm, 28% of the carbon in the fuel was converted into soot.

Line-of-sight averaged temperatures along the flame centreline showed that temperatures decreased with pressure, and the decrease was most pronounced in the lower half of the flame. Temperatures increased at a higher rate at higher pressures along the axial direction, most probably due to the larger amount of

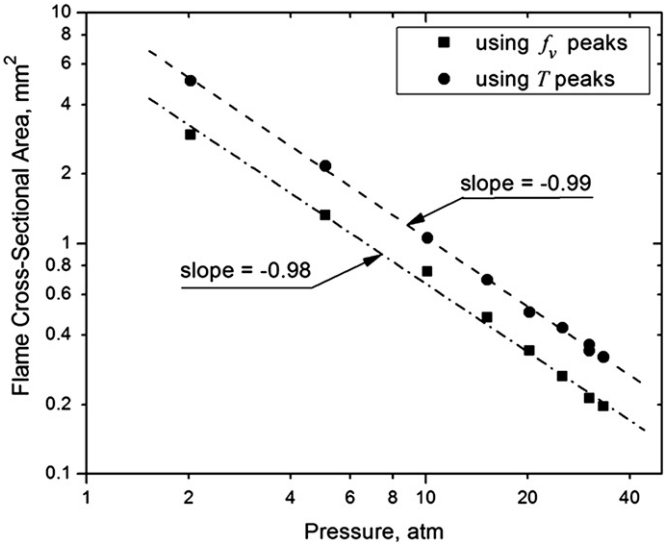

Fig. 9. Dependence of flame cross-sectional area on pressure at 5 mm flame height for ethane–air co-flow laminar diffusion flames. Flame cross-sectional area is calculated from radial peaks of soot volume fraction and temperature. Mass flow rate for carbon in the fuel, $m_c = 0.41$ mg/s. Mass flow rate of ethane, $m_f = 0.52$ mg/s. Measurements were performed using the spectral soot emission technique [63].

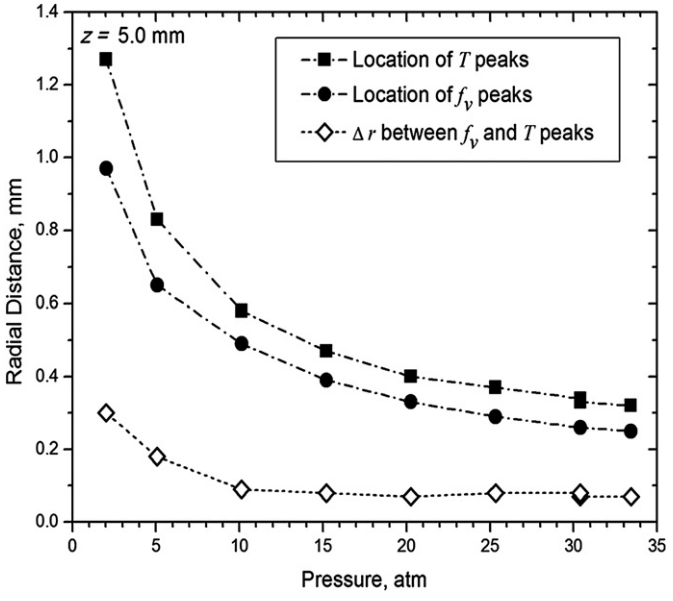

Fig. 11. Variation of the radial locations of the temperature and soot volume fraction peaks as a function of pressure for ethane–air co-flow laminar diffusion flames. Mass flow rate for carbon in the fuel, $m_c = 0.41$ mg/s. Mass flow rate of ethane, $m_f = 0.52$ mg/s. Measurements were performed using the spectral soot emission technique [63].

energy released from the oxidation of a greater amount of soot. At heights except for very low heights and those corresponding to the vicinity of the flame tip, radial temperature gradients stopped increasing at reaching 15 atm, and the trend was reversed at this pressure. The maximum radial temperature gradient was observed as 2000 K/mm at the highest pressure studied.

Joo and Gülder [64] studied ethylene–air flames between 10 atm and 35 atm. The sooting propensity of ethylene is one of the highest in gaseous fuels. In order to avoid transition into smoking flames within the entire pressure range, fuel was diluted with nitrogen of 5 times the fuel volume, and mass flow rate of the fuel was chosen as that carbon mass flow rate could only slightly exceed half of carbon mass flow rate in previous work. Flame height did not change at any pressure, and the cross-sectional area of the flame changed according to $A \propto P^{-1}$. Flames were non-sooting and marginally stable at atmospheric pressure. But, they started producing soot and became increasingly stable as pressure was increased. Maximum line-of-sight integrated soot volume fraction and maximum soot volume fraction scaled with pressure as $P^{1.62}$ and $P^{1.76}$, respectively, for pressures between 10 atm and 30 atm [68]. The scaling corresponds to an increase from 8 ppm at 10 atm to over 62 ppm at 35 atm (see Fig. 8d). Peak carbon conversion scaled with pressure as $P^{1.36}$ between 10 atm and 30 atm and leveled off above 30 atm. A maximum carbon conversion of 6.5% was realized, a rather small percentage for ethylene, but plausible in the presence of extreme dilution. Temperature measurements did not produce anything unexpected. The maximum radial temperature gradient was around 1400 K/mm observed at 30 atm.

In summary, the influence of pressure on the characteristics of co-flow diffusion flames is remarkable, particularly on flame shape and soot concentrations. As pressure is increased, flames become slimmer and increasingly curved inwards. Soot concentrations in a flame increase not only as a consequence of flame narrowing but also because overall soot formation is enhanced. Thus, non-sooting flames at atmospheric pressure can easily transform into sooting flames and furthermore into smoking flames. Flame temperatures are in many cases reduced with increasing pressure due to intensifying radiative heat loss from increasing soot concentrations. As the flame cross-sectional area decreases, density gradients increase. This, along with the contribution of increasing gradients of radiative heat loss due to increasing gradients of soot concentration, leads to an increase in local temperature gradients.

The pressure dependence of soot can generally be simplified in the form of a power law dependence, which becomes less obvious as the pressure range is broadened. Different fuels show different sensitivities to pressure, and thus, their power law fitting exhibits different scaling factors. Fig. 12, originally in [65], shows peak carbon conversion as a function of pressure for flames of methane, ethane, and propane. Curves for different fuels that seem unrelated to each other at first sight conceal a universal pressure dependence. It is explained in [65] that there is a universal behaviour, a single empirical equation that might be extended towards other gaseous hydrocarbon fuels not included in [65]. The analysis is based on three premises: (i) Roper's correlation [66] applies to hydrocarbon flames at high pressure as well. As the inverse pressure dependence of flame cross-sectional area implies, flame height is linearly proportional to the mass flow rate of the fuel. Further, carbon conversion into soot, i.e., soot yield, Y_s, scales with the residence time for non-smoking flames. As a result, soot yield scales with the square root of the mass flow rate of fuel. (ii) For relatively simple aliphatic fuels, soot yield is related to the complexity of the fuel according to $Y_s \propto M$, where M is the molecular mass of the fuel [253,254]. (iii) Peak soot formation rate in diffusion flames scales with the carbon to hydrogen ratio of the fuel [236]. Using these three scaling arguments, it was shown that the data in Fig. 12

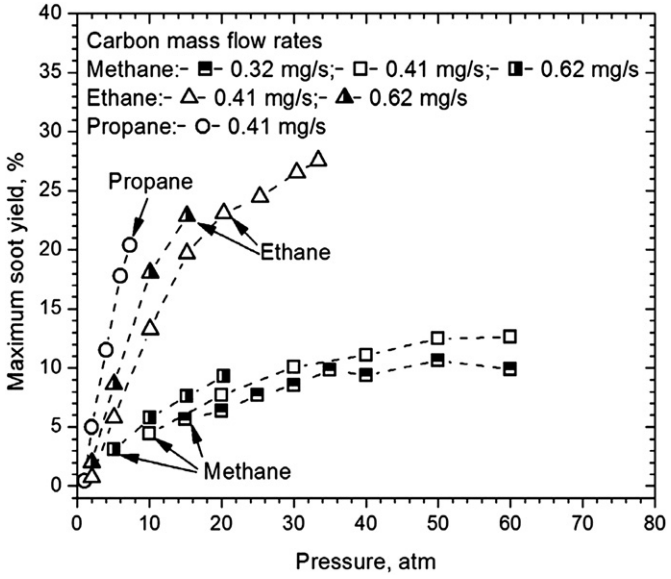

Fig. 12. Maximum carbon conversion into soot of co-flow laminar diffusion flames of methane, ethane, and propane as a function of pressure at different fuel carbon flow rates. Measurements were performed using the spectral soot emission technique [65].

display a unified behaviour with the reduced pressure (pressure divided by the critical pressure of the fuel) [65]. Scaled soot yields (with respect to a reference fuel) as a function of reduced pressure are shown in Fig. 13. The data in Fig. 13 can be presented by an exponential function [65]:

$$\psi = a_0 + a_1 \exp[-a_2 P_r] \tag{13}$$

Here, the coefficients a_0, a_1, and a_2 are specific to the reference fuel chosen. When one of the most studied flames at high pressures, the flame of methane at a flow rate of 0.55 mg/s, is chosen, the coefficients in Eq. (13) are calculated as $a_0 = 15.9$, $a_1 = -16.3$, and $a_2 = 2.65$.

Reduced pressure seems to be a sound correlating parameter because the mass flow rate scaling of soot yield is not uniform over extreme ranges of pressure. Yet, the change in the trend, i.e., due to the dependence of molecular diffusivity on pressure, is similar for

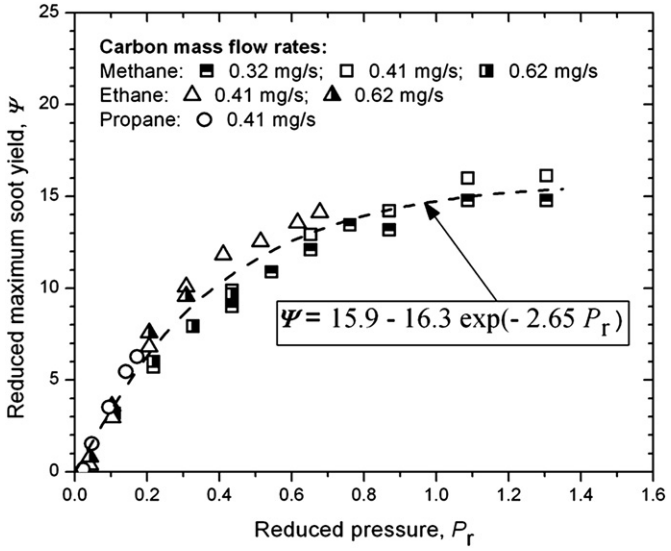

Fig. 13. Unified representation of the variation in maximum carbon conversion with reduced pressure. Dashed line is a least-square curve fit to the data [65].

all hydrocarbon fuels when the pressure is non-dimensionalized by the critical pressure of each fuel. One of the outstanding questions is that whether the soot yield of liquid fuel flames would follow a similar behaviour with pressure.

4. Effect of pressure on soot morphology

Compared to soot concentration, the knowledge of pressure influence on soot morphology is extremely limited. This is partly because optical diagnostics techniques that are used in studying soot morphology are not well established, and the use of intrusive techniques, generally more common in morphology studies, is often not feasible inside of a pressure chamber. Nevertheless, the use of thermophoretic sampling and TEM analysis and the use of LII technique have the potential to provide information on soot morphology change with pressure.

It is well known that soot volume fraction, f_v, soot particle diameter, d_p, and particle number density, N, are related by the equation $f_v = \pi/6\ N d_p^3$. At first glance, this equation suggests that the multiplication of particle number density and particle volume, $\pi/6\ N d_p^3$ term, should increase with pressure as it is known that soot volume fraction increases significantly with pressure. But, the change in flame shape should be included in this consideration that narrowing flame shape forces the particles into a closer space, hence increasing local soot volume fraction. As a result, part of the effect of pressure comes from its influence on flame shape. On the other hand, the fact that soot yield increases with pressure indicates that the rest of the increase in the $\pi/6\ N d_p^3$ term is related to the influence of pressure on the overall rate of soot formation, which is again partly related to flame narrowing since the decomposition of the fuel seems to be closely related to the changes in flame shape and subsequent changes in temperature gradients. For example, Miller and Maahs [38] plotted particle number density as a function of pressure, calculated from their measurements of soot volume fraction and estimation of particle diameter. When particle diameter was assumed to be constant, independent of pressure, and equal to 50 nm, measured soot volume fraction values in their methane–air co-flow diffusion flame suggested over a three order of magnitude increase in particle number density from 2.5 atm to 50 atm.

There have been a few experimental studies that dealt with soot morphology inside the combustion chamber of diesel engines or in the exhaust gases [172,173,207,208,255,256]. Measurements of particle diameter over the engine cycle show mixed results. In one study, particle diameters were found to vary slightly within 30 nm and 50 nm for all crank angles, hence pressures [207]. However, different engine loadings and probe locations result in drastic changes in the trends in mean particle diameter variation with crank angle [208], and particle size distribution is affected by engine loading [172], making comparison between different studies difficult. Furthermore, an increase in mean particle diameter [208] and in count median particle diameter [255], expected at crank angles corresponding to higher pressures, was not realized. Particle diameter measurements in [173] showed that mean particle diameters increased considerably from 11 atm to 21 atm.

Experiments using lab-scale burners provide more consistent results. Milberg [39] analyzed soot particles that deposited on a glass-filter that he used to collect particles for measuring smoking rate. Particle diameters were found to be within 20 nm and 50 nm, and it was reported that particle sizes did not vary with operating conditions (including pressures). In their Wolfhard-Parker slot burner, Flower and Bowman [232] measured soot particle diameter and particle number density in addition to the soot concentration that are summarized in Section 3.2. At a specific height, maximum particle diameter increased from 60 nm at atmospheric pressure to 90 nm at 2 atm. At the same height, particle number density increased significantly except for a tiny radial region. Particles sizes measured by LII technique at pressures between 5 atm and 40 atm show that an increase in particle size with pressure is also present in co-flow diffusion flames [214]. Particle sizing using laser induced incandescence at super-atmospheric pressures is not well established; there are different opinions on LII effectiveness [210,217]. Hofmann et al. [210] compared results from LII system with those from thermophoretic sampling–TEM analysis and reported a satisfactory agreement between these results. The flame was a premixed one, and it was studied between 1 atm and 10 atm. Particle distribution narrowed, and mean particle diameter decreased from atmospheric pressure to 5 atm, and the trends were reversed towards 10 atm. Thermophoretic sampling–TEM analysis was also used for studying co-flow laminar diffusion flames. Kim et al. [178] studied acetylene flames from 0.125 atm to atmospheric pressure and found that mean particle diameter was within 10 nm and 20 nm for all pressures and centreline locations. There was a slight increase in mean particle diameter with pressure at most centreline locations. In a following study [37], ethylene flames were studied, and mean particle diameters were reported as a function of axial location along the centreline. Mean diameters that were between 10 nm and 20 nm for the entire centreline at atmospheric pressure were found to increase to between 30 nm and 40 nm at 8 atm.

5. Modeling of soot formation at elevated pressures

Approaches to modeling soot processes in combustion are summarized in [155]. There have been a few studies that check for model verification at elevated pressures or that focus on the modeling of soot at elevated pressures. Moss et al. [257] developed a semi-empirical model to predict soot volume fraction and number density. The model calculations are based on local mixture fraction, which is obtained by carbon mass fraction measurements by sampling and mass spectroscopy. Measurements were done in a Wolfhard-Parker slot burner at 1 atm and 1.95 atm. Model and experiments agreed on a pressure dependence of peak soot volume fraction according to P^2.

Zhang and Ezekoye [186] performed the first numerical study of soot formation in a laminar co-flow diffusion flame at elevated pressures. A simplified reaction mechanism was used, and soot was modeled based on one species only, acetylene. The simulation predictions were validated at atmospheric pressure. The simulation predicts that soot nucleation, surface growth, agglomeration, and oxidation are enhanced with increasing pressure. The influence of pressure comes mostly from increasing mixture density that combustion gases were constrained in a tighter space at elevated pressures [186]. Particle number density was anticipated to be lower at higher pressures because the increase in particle adhesion dominated over the particle inception; the resultant particles were several times larger. In fact, soot particle diameter was predicted to quadruple from 1 to 4 atm [186].

Kim et al. [37,178] showed that surface growth can be explained by HACA mechanism at sub- and super-atmospheric pressures as well. HACA is usually driven by acetylene, supporting acetylene-based models of soot at elevated pressures. Radiation heat transfer was also enhanced with increasing pressure that radiation surpassed conduction in heating the burner tip and fresh gases from atmospheric pressure to 4 atm [186].

Liu et al. [58] numerically studied methane–air flames that were reported previously in [46]. Similar to [186], they used an acetylene-based chemistry for soot inception and growth but compared two different surface growth possibilities, that are, soot surface growth rate correlates with the soot surface area (model II)

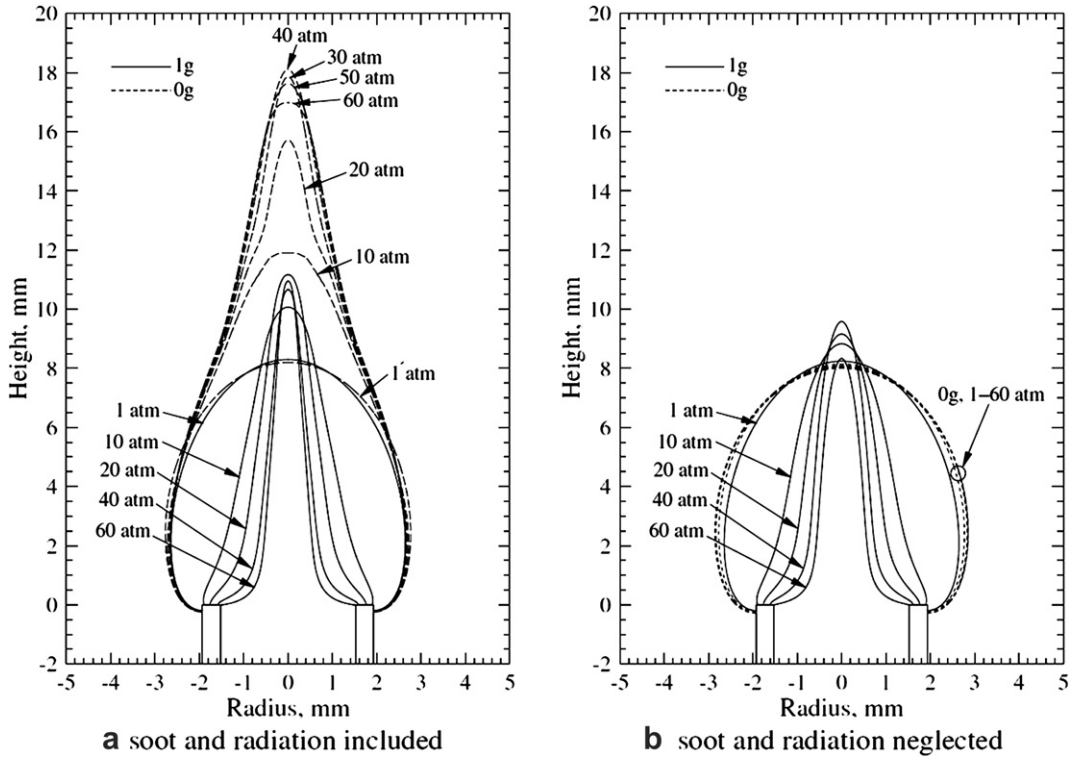

Fig. 14. The effect of pressure and gravity on the stoichiometric mixture fraction surface for methane–air co-flow laminar diffusion flames. Simulations were performed by solving the unmodified and fully-coupled equations governing reactive, compressible, gaseous mixtures which include complex chemistry, detailed radiation heat transfer, and soot formation/oxidation. Soot formation/oxidation was modeled using an acetylene-based, semi-empirical model [258].

or its square root (model I). Flame height calculations using model I predicted only a slight change with pressure and agreed well quantitatively with the experimentally measured flame heights. Same calculations also suggested a pressure influence on flame diameter (calculated based on flame radiation and CH concentration) according to $D \propto P^{-0.5}$. In general, model I was able to capture trends of those observed experimentally more closely than did model II even though model I lacked the quantitative agreement with the experimental data on soot concentrations. For example, model I was successful in predicting scaling relations for the pressure dependence of maximum line-of-sight integrated soot volume fraction and maximum soot volume fraction. The authors [58] reached the same conclusion as [186] that the influence of pressure on soot formation is mostly a physical one arising from

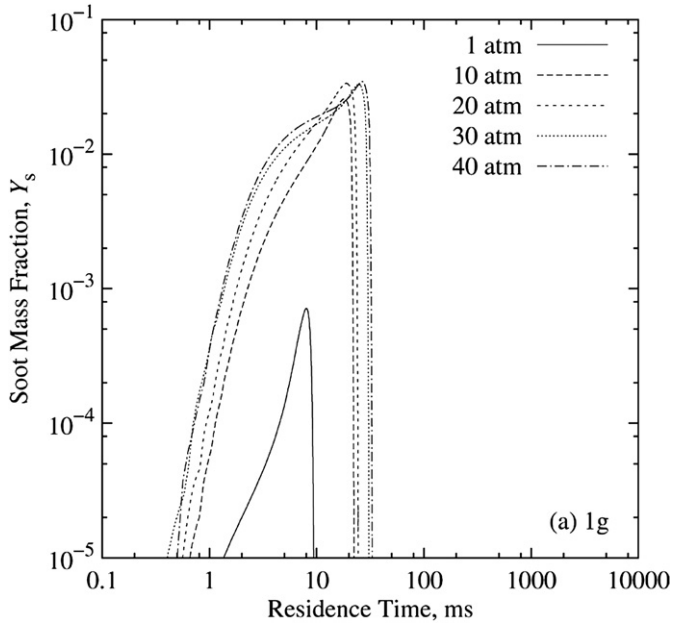

Fig. 15. Soot mass fraction along a soot particle streamline passing through the maximum soot volume fraction for methane–air co-flow laminar diffusion flames. Simulations were performed by solving the unmodified and fully-coupled equations governing reactive, compressible, gaseous mixtures which include complex chemistry, detailed radiation heat transfer, and soot formation/oxidation. Soot formation/oxidation was modeled using an acetylene-based, semi-empirical model [258].

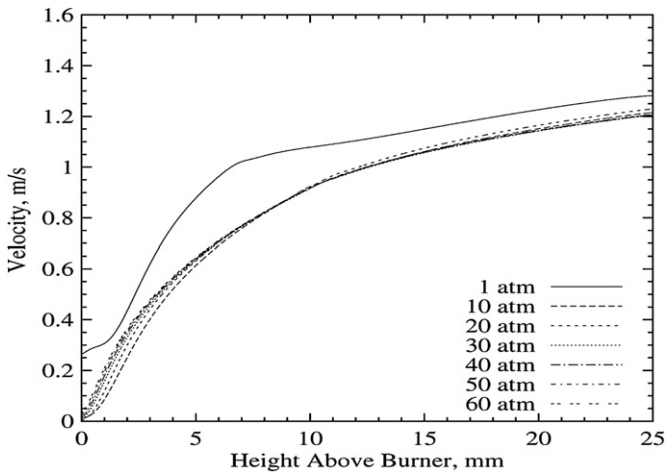

Fig. 16. Distributions of the predicted axial velocity along the flame centerline for methane–air co-flow laminar diffusion flames. Simulations were performed by solving the unmodified and fully-coupled equations governing reactive, compressible, gaseous mixtures which include complex chemistry, detailed radiation heat transfer, and soot formation/oxidation. Soot formation/oxidation was modeled using an acetylene-based, semi-empirical model [258].

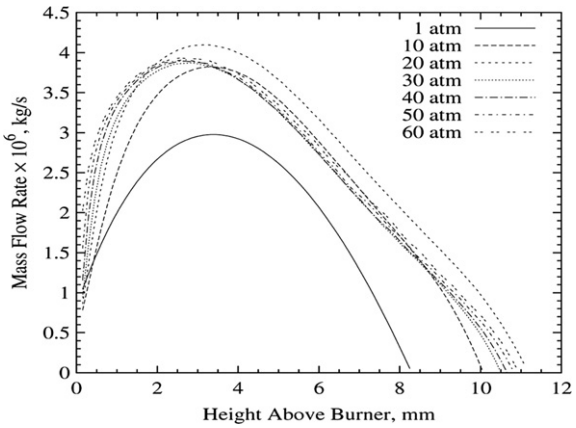

Fig. 17. Distributions of the mass flow rate through the stoichiometric flame envelope for methane–air co-flow laminar diffusion flames. Simulations were performed by solving the unmodified and fully-coupled equations governing reactive, compressible, gaseous mixtures which include complex chemistry, detailed radiation heat transfer, and soot formation/oxidation. Soot formation/oxidation was modeled using an acetylene-based, semi-empirical model [258].

increased mixture density. They also concluded that increasing pressure forces the co-flowing air to infiltrate inwards into the base of the flame [58]. This and the temperature increase at the region of fuel abundance enhance fuel decomposition. Consequently, soot is formed earlier on and in greater quantities in flames at elevated pressures. On the contrary, soot oxidation also takes place earlier in the flame due to the enhanced air entrainment even though later in the flame soot oxidation could be impeded due to reductions in radical concentrations caused by pressure-dependent reactions.

Charest et al. [258] furthered the study of the same flame configuration up to 60 atm adopting model I approach and compared results with the data reported in [40]. Some improvements were made in the model. The computational domain was extended towards the upstream of fuel nozzle to better capture the effect of air entrainment, and the low-Mach-number assumption was abandoned. They simulated burner walls as adiabatic boundaries, and this allowed them to investigate trends above 20 atm [258]. As compared with the study in [58], where soot volume fraction was generally underpredicted, their calculations [258] tended to overpredict soot volume fraction. One of the major differences in the models is that in [58], the temperature at fuel nozzle surface was taken as 300 K whereas in [258], it was adiabatic, i.e., the same temperature as the fuel stream. Both studies [58,258] gave correct trends in soot fractions and flame heights in agreement with the experimental results.

Flame shapes for zero- and normal-gravity flames predicted in [258] are illustrated in Fig. 14; it is seen that flame shapes are almost identical at 0 g and 1 g at atmospheric pressure, where buoyancy forces are not as significant. As pressure increases however, buoyancy forces that are present at 1 g confine the inner flow into a narrower space. When soot formation and oxidation reactions, and radiation heat exchange were turned off, the simulations predict similar flame heights (defined by the stoichiometric mixture fraction surface) for zero gravity and normal-gravity flames at all pressures, Fig. 14b. Residence times in these diffusion flames are assumed to be independent of pressure when the mass flow rate is kept constant. However, simulations indicate that residence time depends on pressure between 1 atm and 10 atm as shown in Fig. 15. In this pressure range, the flame is said to be not fully developed because soot-region still extends towards the fuel nozzle and axial velocity decreases with increasing pressure (see Fig. 16), increasing residence time of soot. The degree of air entrainment can be judged from profiles of mass flow rate through the flame surface, Fig. 17. Constancy of the residence times at pressures between 10 and 60 atm is apparent in Fig. 17. It seems that the air entrainment into the flame increases from atmospheric to 10 atm, but beyond 10 atm it is almost constant, Fig. 17.

Similar simulations were done on pure [259] and nitrogen-diluted [62] ethylene flames by Groth and co-workers. Measured and numerically predicted soot volume fraction maps of the nitrogen-diluted ethylene co-flow laminar diffusion flames up to 35 atm are shown in Fig. 18. It is seen that flame shape (based on soot concentration) is well predicted. Many trends regarding the effect of pressure on soot concentration were also accurately predicted, even though quantitative agreement is poor in soot volume fraction that the model overpredicts maximum soot volume fraction. The model [62] explains the reduced sensitivity of soot formation to pressure at elevated pressures as being a result of the reduced availability of precursors. In Fig. 19, it is clearly seen that the region of ethylene decomposition into acetylene moves towards into the fuel tube as pressure is increased, and the peak concentration of acetylene reduces with pressure. Even though in reality many more species other than acetylene take part in the soot formation process, the same possibly applies to all species that are consumed during soot production. As pressure increases, conversion of the carbon in the fuel to soot approaches to what is available from existing building blocks, leaving less room for further

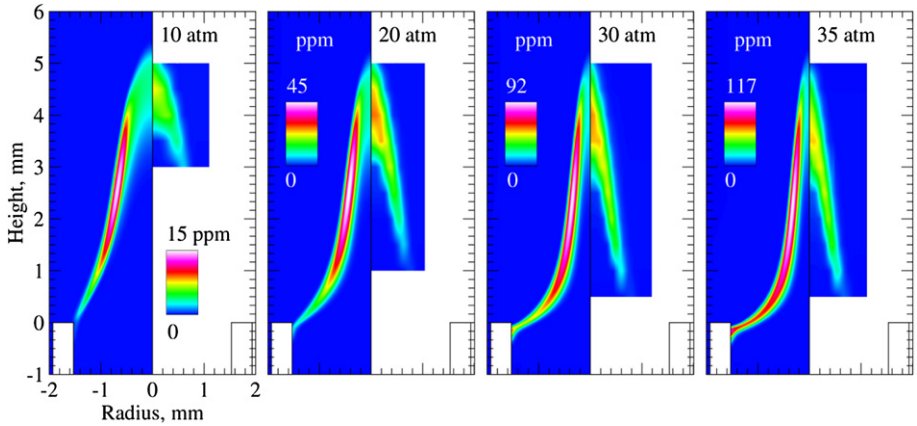

Fig. 18. Predicted (left) and measured (right) contours for soot volume fraction. Measurements were performed using the spectral soot emission technique, and simulations were performed by solving the unmodified and fully-coupled equations governing reactive, compressible, gaseous mixtures which include complex chemistry, detailed radiation heat transfer, and soot formation/oxidation. Soot formation/oxidation was modeled using an acetylene-based, semi-empirical model [62].

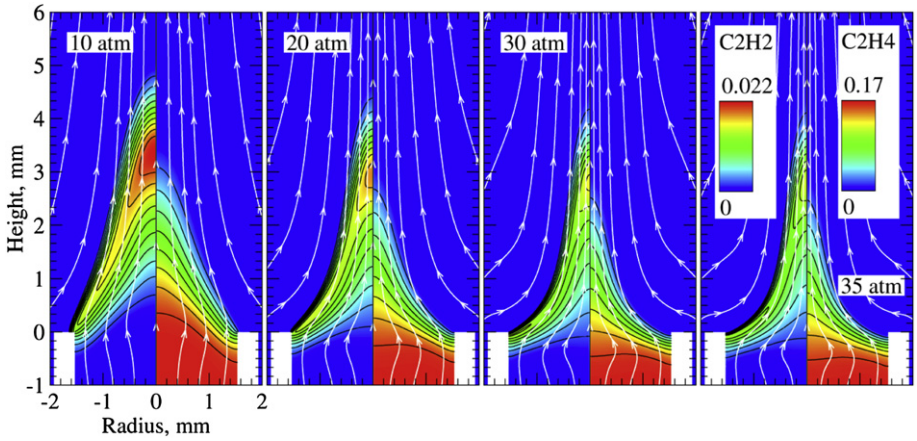

Fig. 19. Model predictions for C_2H_2 (left) and C_2H_4 (right) mass fraction. Simulations were performed by solving the unmodified and fully-coupled equations governing reactive, compressible, gaseous mixtures which include complex chemistry, detailed radiation heat transfer, and soot formation/oxidation. Soot formation/oxidation was modeled using an acetylene-based, semi-empirical model [62].

conversion. The model also suggests that soot formation rates do not change significantly with pressure; the increase in soot yield comes from increasing time spent on soot formation, that is, soot inception starts earlier (following the particle streamline passing through peak soot concentration), and ultimate soot destruction occurs later as pressure is increased [259].

6. Conclusions

Despite the fact that the pressure significantly influences soot formation, our insight into the effect of pressure on formation of soot is very limited. There seems to be no reliable method of scaling the extensive experimental data obtained at atmospheric pressure to elevated pressures. Information on soot formation in laminar flames, obtained at elevated pressures, has the potential to shed light on turbulent diffusion flames encountered in practical applications by exploiting the similarities between laminar and turbulent flames. However, there is no data on the sooting behaviour of liquid fuels in tractable laminar diffusion flames at pressures corresponding to the operation of gas turbine and reciprocating engines: most data, if not all, are at atmospheric pressure. There is no reliable information about the size and morphology of particulates at high pressures. Existing few studies on primary particle size dependence on pressure are contradictory. It is not known whether the particle size and morphology are fuel dependent. The major impediment to measuring size and morphology at elevated pressures seems to be a lack of non-intrusive diagnostics that could perform reliable measurements. Size and morphology information is essential for radiation modelling and diagnostics purposes.

Smoke point fuel mass flow rate decreases with increasing pressure. For tractable measurements to assess the effect of pressure, the fuel mass flow rate at all pressures should be kept constant, and this mass flow rate should be equal or less than the smoke point fuel mass flow rate at the highest pressure considered. For soot concentrations at high pressures, LII and SSE yield reliable measurements. Reliable soot concentration measurements with LOSA should be limited to pressures lower than 10 atm due to severe beam steering. Soot particle size measurements with LII above 10 atm are not as reliable as those at lower pressures.

Available high pressure soot yield data from aliphatic gaseous diffusion flames seem to display a unified dependence on pressure when the soot yield is properly normalized. There are three important aspects of this unified behaviour: (1) the soot yield of gaseous fuels display a unified dependence on pressure, at least for aliphatic ones; (2) the soot yield seems to reach a plateau asymptotically; and (3) when combined with the characteristic time scales and histories of soot particles, these soot yield behaviour may constitute the basis of relatively simple soot models for turbulent combustion codes. What is unknown currently is whether the liquid fuels, more precisely pure liquid hydrocarbons, display a similar unified behaviour.

The very brief discussion of the soot formation and oxidation given in this review indicates that the state of the art is not yet at a level to be able to achieve sound predictions of soot formation and oxidation in flames from the first principles using numerical simulation, especially at elevated pressures. The main drawback is that not all elementary reaction rate coefficients are available.

Acknowledgements

The authors wish to thank K. A. Thomson, D. S. Bento, P. M. Mandatori, H. I. Joo, M. E. Vaillancourt, and G. Intasopa who performed most of the experiments included in this review as parts of their dissertations. Numerical simulations of some of the flames at elevated pressures were performed by M. R. J. Charest, to whom we also owe our thanks.

Operational funds for the work performed in the senior author's laboratory and reviewed in this paper have been provided partially by Natural Sciences and Engineering Research Council (NSERC) and Canadian Space Agency (CSA). We acknowledge an infrastructure grant provided by Canadian Foundation for Innovation (CFI) for building the high pressure soot rig at UTIAS.

References

[1] Aristotle. The works of Aristotle: the famous Philosopher. Penn State Electronic Classics Series Publication; 2005.
[2] Boyland E. The toxicology of soot. In: Lahaye J, Prado G, editors. Soot in combustion systems and its toxic properties. New York: Plenum Press; 1983. p. 13–24.
[3] Curtis L, Rea W, Smith-Willis P, Fenyves E, Pan Y. Adverse health effects of outdoor air pollutants. Environ Int 2006;32:815–30.
[4] Kennedy IM. The health effects of combustion-generated aerosols. Proc Combust Inst 2007;31:2757–70.
[5] Kaiser J. Evidence mounts that tiny particles can kill. Science 2000;289:22–3.
[6] BéruBé K, Balharry D, Sexton K, Koshy L, Jones T. Combustion-derived nanoparticles: mechanisms of pulmonary toxicity. Clin Exp Pharmacol Physiol 2007;34:1044–50.
[7] Samet JM, Dominici F, Curriero FC, Coursac I, Zeger SL. Fine particulate air pollution and mortality in 20 U.S. cities, 1987–1994. New Engl J Med 2000; 343:1742–9.
[8] Kaden DA, Hites RA, Thilly WG. Mutagenicity of soot and associated polycyclic aromatic hydrocarbons to *salmonella typhimurium*. Cancer Res 1979; 39:4152–9.

[9] Brockmann M, Fischer M, Müller KM. Exposure to carbon black: a cancer risk? Int Arch Occ Environ Hea 1998;71:85–99.
[10] Kumfer B, Kennedy I. The role of soot in the health effects of inhaled airborne particles. In: Bockhorn H, D'Anna A, Sarofim AF, Wang H, editors. Combustion generated fine carbonaceous particles (proceedings of an international workshop held in Villa Orlandi, Anacapri, May 13–16, 2007). KIT Scientific Publishing; 2009. p. 1–15.
[11] US Environmental Protection Agency. Clean air act. Federal register (P.L. 88–206); 1963.
[12] US Environmental Protection Agency. Clean air act—amendments. Federal register (P.L. 91–604); 1970.
[13] US Environmental Protection Agency. Clean air act—amendments. Federal register (P.L. 101–549); 1990.
[14] The European Parliament and the Council of the European Union. Directive 2008/50/EC on ambient air quality and cleaner air for Europe. Off J Eur Union; 2008.
[15] Environmental Canada. Canadian environmental protection act. Canada Gazette—Gazette du Canada; 1999.
[16] Charlson RJ, Schwartz SE, Hales JM, Cess RD, Coakley Jr JA, Hansen JE, et al. Climate forcing by anthropogenic aerosols. Science 1992;255:423–30.
[17] Shaddix CR, Williams TC. Soot: giver and taker of light. Am Sci 2007;95:232–9.
[18] Kärcher B, Möhler O, DeMott PJ, Pechtl S, Yu F. Insights into the role of soot aerosols in cirrus cloud formation. Atmos Chem Phys 2007;7:4203–27.
[19] Hendricks J, Kärcher B, Lohmann U, Ponater M. Do aircraft black carbon emissions affect cirrus clouds on the global scale? Geophys Res Lett 2005;32:1–4.
[20] Gorbunov B, Baklanov A, Kakutkina N, Windsor HL, Toumi R. Ice nucleation on soot particles. J Aerosol Sci 2001;32:199–215.
[21] DeMott PJ, Chen Y, Kreidenweis SM, Rogers DC, Sherman DE. Ice formation by black carbon particles. Geophys Res Lett 1999;26:2429–32.
[22] Penner JE. Effects of soot aerosols from aircraft on cirrus cloud. UTIAS-MITACS international workshop on aviation and climate change; 2008.
[23] Hansen JE. Can we defuse the global warming time bomb? [retrieved April 2011], http://pubs.giss.nasa.gov/docs/2003/2003_Hansen.pdf; 2003.
[24] Hansen JE, Nazarenko L. Soot climate forcing via snow and ice albedos. Proc Natl Acad Sci USA 2004;101:423–8.
[25] Andreae MO. The dark side of aerosols. Nature 2001;409:671–2.
[26] Faraday M. The chemical history of a candle. New York: Dover; 2002.
[27] Lefebvre AH, Ballal DR. Gas turbine combustion: alternative fuels and emissions. 3rd ed. CRC Press; 2010.
[28] Sutton GP. History of liquid propellant rocket engines. AIAA; 2006.
[29] Faeth GM. Laminar and turbulent gaseous diffusion flames. In: Ross HD, editor. Microgravity combustion: fire in free fall. Academic Press; 2001. p. 83–182.
[30] Moss JB. Turbulent diffusion flames. In: Cox G, editor. Combustion fundamentals of fire. London: Academic Press; 1995. p. 221–72.
[31] Cavaliere A, Ragucci R. Gaseous diffusion flames: simple structures and their interaction. Prog Energy Combust 2001;27:547–85.
[32] Glassman I, Yetter RA. Combustion. 4th ed. Academic Press; 2008.
[33] Kent JH. Carbon formation in laminar and turbulent diffusion flames. In: Jander H, Wagner HG, editors. Soot formation in combustion—an international round table discussion. Göttingen: Vandenhoeck & Ruprecht; 1990. p. 41–66.
[34] Gülder ÖL. Soot formation in laminar diffusion flames at elevated temperatures. Combust Flame 1992;88:75–82.
[35] Hu B, Yang B, Köylü ÜÖ. Soot measurements at the axis of an ethylene/air non-premixed turbulent jet flame. Combust Flame 2003;134:93–106.
[36] Yang B, Köylü ÜÖ. Detailed soot field in a turbulent non-premixed ethylene/air flame from laser scattering and extinction experiments. Combust Flame 2005;141:55–65.
[37] Kim CH, Xu F, Faeth GM. Soot surface growth and oxidation at pressures up to 8.0 atm in laminar non-premixed and partially premixed flames. Combust Flame 2008;152:301–16.
[38] Miller IM, Maahs HG. High pressure flame system for pollution studies with results for methane–air diffusion flames. Tech. Rep. TN D-8407; NASA; 1977.
[39] Milberg ME. Carbon formation in an acetylene–air diffusion flame. J Phys Chem 1959;63:578–82.
[40] Joo HI, Gülder ÖL. Soot formation and temperature field structure in co-flow laminar methane–air diffusion flames at pressures from 10 to 60 atm. Proc Combust Inst 2009;32:769–75.
[41] Parker WG, Wolfhard HG. Carbon formation in flames. J Chem Soc; 1950:2038–49.
[42] Diederichsen J, Wolfhard HG. Spectrographic examination of gaseous flames at high pressure. Proc R Soc Lond A 1956;236:89–103.
[43] Mandatori PM, Gülder ÖL. Complete conversion of ethane to soot in a coflow laminar diffusion flame at 3.65 MPa. Combust Flame 2007;150:400–3.
[44] McCrain LL, Roberts WL. Measurements of the soot volume field in laminar diffusion flames at elevated pressures. Combust Flame 2005;140:60–9.
[45] Sato J. Extinction of counterflow diffusion flame in high pressures. Combust Sci Technol 1991;75:103–13.
[46] Thomson KA, Gülder ÖL, Weckman EJ, Fraser RA, Smallwood GJ, Snelling DR. Soot concentration and temperature measurements in co-annular, non-premixed CH_4/air laminar flames at pressures up to 4 MPa. Combust Flame 2005;140:222–32.
[47] Sung CJ, Li B, Wang H, Law CK. Structure and sooting limits in counterflow methane/air and propane/air diffusion flames from 1 to 5 atmospheres. Proc Combust Inst 1998;27:1523–9.
[48] Du DX, Wang H, Law CK. Soot formation in counterflow ethylene diffusion flames from 1 to 2.5 atmospheres. Combust Flame 1998;113:264–70.
[49] Du DX, Axelbaum RL, Law CK. Experiments on the sooting limits of aerodynamically-strained diffusion flames. Proc Combust Inst 1989;22:387–94.
[50] Wehrmeyer JA, Yeralan S, Tecu KS. Influence of strain rate and fuel dilution on laminar non-premixed hydrogen–air flame structure: an experimental investigation. Combust Flame 1996;107:125–40.
[51] Sung CJ, Liu JB, Law CK. Structural response of counterflow diffusion flames to strain rate variations. Combust Flame 1995;102:481–92.
[52] Yamamoto M, Duan S, Senkan S. The effect of strain rate on polycyclic aromatic hydrocarbon (PAH) formation in acetylene diffusion flames. Combust Flame 2007;151:532–41.
[53] Flower WL, Bowman CT. Soot production in axisymmetric laminar diffusion flames at pressures from one to ten atmospheres. Proc Combust Inst 1988;21:1115–24.
[54] Flower WL. Soot particle temperatures in axisymmetric laminar ethylene–air diffusion flames at pressures up to 0.7 MPa. Combust Flame 1989;77:279–93.
[55] Lee W, Na YD. Soot study in laminar diffusion flames at elevated pressure using two-pyrometry and Abel inversion. JSME Int J Ser B 2000;43:550–5.
[56] Bento DS, Thomson KA, Gülder ÖL. Soot formation and temperature field structure in laminar propane–air diffusion flames at elevated pressures. Combust Flame 2006;145:765–78.
[57] Berry TL, Roberts WL. Measurement of smoke point in velocity-matched coflow laminar diffusion flames with pure fuels at elevated pressures. Combust Flame 2006;145:571–8.
[58] Liu F, Thomson KA, Guo H, Smallwood GJ. Numerical and experimental study of an axisymmetric coflow laminar methane–air diffusion flame at pressures between 5 and 40 atmospheres. Combust Flame 2006;146:456–71.
[59] Berry Yelverton TL, Roberts WL. Soot surface temperature measurements in pure and diluted flames at atmospheric and elevated pressures. Exp Therm Fluid Sci 2008;33:17–22.
[60] Joo HI, Gülder ÖL. Soot formation and temperature structure in small methane–oxygen diffusion flames at subcritical and supercritical pressures. Combust Flame 2010;157:1194–201.
[61] Joo HI, Gülder ÖL. Observation of liquid phase material in methane–air laminar diffusion flame soot experiments above 60 atmospheres. Combust Flame 2010;157:408–9.
[62] Charest MRJ, Joo HI, Gülder ÖL, Groth CPT. Experimental and numerical study of soot formation in laminar ethylene diffusion flames at elevated pressures from 10 to 35 atm. Proc Combust Inst 2011;33:549–57.
[63] Mandatori PM, Gülder ÖL. Soot formation in laminar ethane diffusion flames at pressures from 0.2 to 3.3 MPa. Proc Combust Inst 2011;33:577–84.
[64] Joo HI, Gülder ÖL. Experimental study of soot and temperature field structure of laminar co-flow ethylene–air diffusion flames with nitrogen dilution at elevated pressures. Combust Flame 2011;158:416–22.
[65] Gülder ÖL, Intasopa G, Joo HI, Mandatori PM, Bento DS, Vaillancourt ME. Unified behaviour of maximum soot yields of methane, ethane and propane laminar diffusion flames at high pressures. Combust Flame 2011;158:2037–44.
[66] Roper FG. The prediction of laminar jet diffusion flame sizes: part I. Theoretical model. Combust Flame 1977;29:219–26.
[67] Burke SP, Schumann TEW. Diffusion flames. Ind Eng Chem Res 1928;20:998–1004.
[68] Joo HI. Soot formation in non-premixed laminar flames at subcritical and supercritical pressures. Ph.D. thesis; University of Toronto; 2010.
[69] Savaş Ö, Gollahalli SR. Stability of lifted laminar round gas-jet flame. J Fluid Mech 1986;165:297–318.
[70] Chung SH, Lee BJ. On the characteristics of laminar lifted flames in a non-premixed jet. Combust Flame 1991;86:62–72.
[71] Prasad K, Price EW. A numerical study of the leading edge of laminar diffusion flames. Combust Flame 1992;90:155–73.
[72] Lee BJ, Chung SH. Stabilization of lifted tribrachial flames in a laminar non-premixed jet. Combust Flame 1997;109:163–72.
[73] Takahashi F, Schmoll WJ, Katta VR. Attachment mechanisms of diffusion flames. Proc Combust Inst 1998;27:675–84.
[74] Won SH, Chung SH, Cha MS, Lee BJ. Lifted flame stabilization in developing and developed regions of coflow jets for highly diluted propane. Proc Combust Inst 2000;28:2093–9.
[75] Chung SH. Stabilization, propagation and instability of tribrachial triple flames. Proc Combust Inst 2007;31:877–92.
[76] Tsuji H. Counterflow diffusion flames. Prog Energy Combust 1982;8:93–119.
[77] Ikeda Y, Beduneau JL. Attachment structure of a non-premixed laminar methane flame. Proc Combust Inst 2005;30:391–8.
[78] Panek N, Charest MRJ, Gülder ÖL. Simulation of microgravity diffusion flames using sub-atmospheric pressures. AIAA J 2012;26:2191–7.
[79] Intasopa G. Soot measurements in high pressure diffusion flames of gaseous and liquid fuels. Master's thesis; University of Toronto; 2011.
[80] de Andrade Oliveira MH, Luijten CCM, de Goey LPH. Soot measurements in laminar flames of gaseous and (prevaporized) liquid fuels. Proceedings of the European Combustion Meeting; 2009.
[81] Wang H. Formation of nascent soot and other condensed-phase materials in flames. Proc Combust Inst 2011;33:41–67.
[82] Maricq MM. Electrical mobility based characterization of bimodal soot size distributions in rich premixed flames. In: Bockhorn H, D'Anna A, Sarofim AF, Wang H, editors. Combustion generated fine carbonaceous particles

(proceedings of an international workshop held in Villa Orlandi, Anacapri, May 13–16, 2007). KIT Scientifc Publishing; 2009. p. 347–66.
[83] Wang H, Abid A. Size distribution and chemical composition of nascent soot formed in premixed ethylene flames. In: Bockhorn H, D'Anna A, Sarofim AF, Wang H, editors. Combustion generated fine carbonaceous particles (proceedings of an international workshop held in Villa Orlandi, Anacapri, May 13–16, 2007). KIT Scientifc Publishing; 2009. p. 367–84.
[84] Palmer HB, Cullis CF. The formation of carbon from gases. In: Walker Jr. PL, editor. Chemistry and physics of carbon, vol. 1. New York: Marcel Dekker; 1965. p. 265–325.
[85] Dobbins RA, Subramaniasivam H. Soot precursor particles in flames. In: Bockhorn H, editor. Soot formation in combustion: mechanisms and models. Berlin: Springer; 1994. p. 290–301.
[86] Vander Wal RL, Tomasek AJ, Ticich TM. Synthesis, laser processing, and flame purification of nanostructured carbon. Nano Lett 2003;3:223–9.
[87] Smith OI. Fundamentals of soot formation in flames with application to diesel engine particulate emissions. Prog Energy Combust 1981;7:275–91.
[88] Clague ADH, Donnet JB, Wang TK, Peng JCM. A comparison of diesel engine soot with carbon black. Carbon 1999;37:1553–65.
[89] Wang H, Frenklach M. Transport properties of polycyclic aromatic hydrocarbons for flame modeling. Combust Flame 1994;96:163–70.
[90] Böhm H, Jander H. PAH formation in acetylene–benzene pyrolysis. Phys Chem Chem Phys 1999;1:3775–81.
[91] Weilmünster P, Keller A, Homann KH. Large molecules, radicals, ions, and small soot particles in fuel-rich hydrocarbon flames part I: positive ions of polycyclic aromatic hydrocarbons (PAH) in low-pressure premixed flames of acetylene and oxygen. Combust Flame 1999;116:62–83.
[92] Griesheimer J, Homann KH. Large molecules, radicals ions, and small soot particles in fuel-rich hydrocarbon flames part II. Aromatic radicals and intermediate PAHs in a premixed low-pressure naphthalene/oxygen/argon flame. Proc Combust Inst 1998;27:1753–9.
[93] Ahrens J, Keller A, Kovacs R, Homann KH. Large molecules, radicals, ions, and small soot particles in fuel-rich hydrocarbon flames: part III: REMPI mass spectrometry of large flame PAHs and fullerenes and their quantitative calibration through sublimation. Berich Bunsen Gesell 1998;102: 1823–39.
[94] Violi A. Modeling of soot particle inception in aromatic and aliphatic premixed flames. Combust Flame 2004;139:279–87.
[95] Keller A, Kovacs R, Homann KH. Large molecules, ions, radicals and small soot particles in fuel-rich hydrocarbon flames part IV. Large polycyclic aromatic hydrocarbons and their radicals in a fuel-rich benzene–oxygen flame. Phys Chem Chem Phys 2000;2:1667–75.
[96] Slavinskaya NA, Braun-Unkhoff M, Frank P. Modeling of PAH and polyyne formation in premixed atmospheric flames C_2H_4/air. Proceedings of the European combustion meeting; 2005.
[97] Richter H, Granata S, Green WH, Howard JB. Detailed modeling of PAH and soot formation in a laminar premixed benzene/oxygen/argon low-pressure flame. Proc Combust Inst 2005;30:1397–405.
[98] Öktem B, Tolocka MP, Zhao B, Wang H, Johnston MV. Chemical species associated with the early stage of soot growth in a laminar premixed ethylene–oxygen–argon flame. Combust Flame 2005;142:364–73.
[99] Mathieu O, Frache G, Djebaïli-Chaumeix N, Paillard CE, Krier G, Muller JF, et al. Characterization of adsorbed species on soot formed behind reflected shock waves. Proc Combust Inst 2007;31:511–9.
[100] D'Anna A, D'Alessio A, Minutolo P. Spectroscopic and chemical characterization of soot inception processes in premixed laminar flames at atmospheric pressure. In: Bockhorn H, editor. Soot formation in combustion: mechanisms and models. Berlin: Springer; 1994. p. 83–103.
[101] Frenklach M, Clary DW, Gardiner Jr WC, Stein SE. Detailed kinetic modeling of soot formation in shock pyrolysis of acetylene. Proc Combust Inst 1985;20: 887–901.
[102] Frenklach M, Warnatz J. Detailed modeling of PAH profiles in a sooting low-pressure acetylene flame. Combust Sci Technol 1987;51:265–83.
[103] Westmoreland PR, Dean AM, Howard JB, Longwell JP. Forming benzene in flames by chemically activated isomerization. J Phys Chem 1989;93:8171–80.
[104] Frenklach M, Wang H. Detailed mechanism and modeling of soot particle formation. In: Bockhorn H, editor. Soot formation in combustion: mechanisms and models. Berlin: Springer; 1994. p. 162–90.
[105] Colket MB, Hall RJ. Successes and uncertainties in modeling soot formation in laminar, premixed flames. In: Bockhorn H, editor. Soot formation in combustion: mechanisms and models. Berlin: Springer; 1994. p. 442–70.
[106] Melius CF, Colvin ME, Marinov NM, Pitz WJ, Senkan SM. Reaction mechanisms in aromatic hydrocarbon formation involving the C_5H_5 cyclopentadienyl moiety. Proc Combust Inst 1996;26:685–92.
[107] Wang H, Frenklach M. A detailed kinetic modeling study of aromatics formation in laminar premixed acetylene and ethylene flames. Combust Flame 1997;110:173–221.
[108] Haynes BS, Wagner HG. Soot formation. Prog Energy Combust 1981;7:229–73.
[109] Homann KH. Formation of large molecules, particulates and ions in premixed hydrocarbon flames; progress and unresolved questions. Proc Combust Inst 1985;20:857–70.
[110] Howard JB. Carbon addition and oxidation reactions in heterogeneous combustion and soot formation. Proc Combust Inst 1991;23:1107–27.
[111] Frenklach M. Reaction mechanism of soot formation in flames. Phys Chem Chem Phys 2002;4:2028–37.
[112] Shukla B, Susa A, Miyoshi A, Koshi M. In situ direct sampling mass spectrometric study on formation of polycyclic aromatic hydrocarbons in toluene pyrolysis. J Phys Chem A 2007;111:8308–24.
[113] Schuetz CA, Frenklach M. Nucleation of soot: molecular dynamics simulations of pyrene dimerization. Proc Combust Inst 2002;29:2307–14.
[114] Skjøth-Rasmussen MS, Glarborg P, Østberg M, Johannessen JT, Livbjerg H, Jensen AD, et al. Formation of polycyclic aromatic hydrocarbons and soot in fuel-rich oxidation of methane in a laminar flow reactor. Combust Flame 2004;136:91–128.
[115] Colket MB, Seery DJ. Reaction mechanisms for toluene pyrolysis. Proc Combust Inst 1994;25:883–91.
[116] Mukherjee J, Sarofim AF, Longwell JP. Polycyclic aromatic hydrocarbons from the high-temperature pyrolysis of pyrene. Combust Flame 1994;96:191–200.
[117] Bockhorn H, Fetting F, Wenz HW. Investigation of the formation of high molecular hydrocarbons and soot in premixed hydrocarbon-oxygen flames. Berich Bunsen Gesell 1983;87:1067–73.
[118] Dobbins RA, Fletcher RA, Chang HC. The evolution of soot precursor particles in a diffusion flame. Combust Flame 1998;115:285–98.
[119] Dobbins RA, Fletcher RA, Lu W. Laser microprobe analysis of soot precursor particles and carbonaceous soot. Combust Flame 1995;100:301–9.
[120] Bittner JD, Howard JB. Composition profiles and reaction mechanisms in a near-sooting premixed benzene/oxygen/argon flame. Proc Combust Inst 1981;8:1105–16.
[121] Weissman M, Benson SW. Mechanism of soot initiation in methane systems. Prog Energy Combust 1989;15:273–85.
[122] Cole JA, Bittner JD, Longwell JP, Howard JB. Formation mechanisms of aromatic compounds in aliphatic flames. Combust Flame 1984;56:51–70.
[123] Smith RD. A direct mass spectrometric study of the mechanism of toluene pyrolysis at high temperatures. J Phys Chem 1979;83:1553–63.
[124] Smith RD. Formation of radicals and complex organic compounds by high-temperature pyrolysis: the pyrolysis of toluene. Combust Flame 1979;35: 179–90.
[125] D'Anna A, Violi A. Detailed modeling of the molecular growth process in aromatic and aliphatic premixed flames. Energy Fuel 2005;19:79–86.
[126] D'Anna A, Violi A, D'Alessio A, Sarofim AF. A reaction pathway for nanoparticle formation in rich premixed flames. Combust Flame 2001;127:1995–2003.
[127] Frenklach M, Clary DW, Gardiner Jr WC, Stein SE. Effect of fuel structure on pathways to soot. Proc Combust Inst 1988;21:1067–76.
[128] Bruinsma OSL, Moulijn JA. The pyrolytic formation of polycyclic aromatic hydrocarbons from benzene, toluene, ethylbenzene, styrene, phenylacetylene and n-decane in relation to fossil fuels utilization. Fuel Process Technol 1988;18:213–36.
[129] Miller JA, Melius CF. Kinetic and thermodynamic issues in the formation of aromatic compounds in flames of aliphatic fuels. Combust Flame 1992;91: 21–39.
[130] Pope CJ, Miller JA. Exploring old and new benzene formation pathways in low-pressure premixed flames of aliphatic fuels. Proc Combust Inst 2000;28: 1519–27.
[131] Marinov NM, Castaldi MJ, Melius CF, Tsang W. Aromatic and polycyclic aromatic hydrocarbon formation in a premixed propane flame. Combust Sci Technol 1997;128:295–342.
[132] Hansen N, Cool TA, Westmoreland PR, Kohse-Höinghaus K. Recent contributions of flame-sampling molecular-beam mass spectrometry to a fundamental understanding of combustion chemistry. Prog Energy Combust 2009; 35:168–91.
[133] Hansen N, Miller JA, Westmoreland PR, Kasper T, Kohse-Höinghaus K, Wang J, et al. Isomer-specific combustion chemistry in allene and propyne flames. Combust Flame 2009;156:2153–64.
[134] Homann KH, Wagner HG. Chemistry of carbon formation in flames. Proc R Soc Lond A 1968;307:141–52.
[135] Sarofim AF, Longwell JP, Wornat MJ, Mukherjee J. The role of biaryl reactions in PAH and soot formation. In: Bockhorn H, editor. Soot formation in combustion: mechanisms and models. Berlin: Springer; 1994. p. 485–99.
[136] Karataş AE, Commodo M, Gülder ÖL. Soot formation in co- and counter-flow laminar diffusion flames of binary mixtures of ethylene and butane isomers and synergistic effects. Energy Fuel 2010;24:4912–8.
[137] Markatou P, Wang H, Frenklach M. A computational study of sooting limits in laminar premixed flames of ethane, ethylene, and acetylene. Combust Flame 1993;93:467–82.
[138] Astholz DC, Durant J, Troe J. Thermal decomposition of toluene and of benzyl radicals in shock waves. Proc Combust Inst 1981;8:885–92.
[139] Apicella B, Carpentieri A, Alfè M, Barbella R, Tregrossi A, Pucci P, et al. Mass spectrometric analysis of large PAH in a fuel-rich ethylene flame. Proc Combust Inst 2007;31:547–53.
[140] Sivaramakrishnan R, Tranter RS, Brezinsky K. A high pressure model for the oxidation of toluene. Proc Combust Inst 2005;30:1165–73.
[141] Kazakov A, Wang H, Frenklach M. Detailed modeling of soot formation in laminar premixed ethylene flames at a pressure of 10 bar. Combust Flame 1995;100:111–20.
[142] Frenklach M, Clary DW, Yuan T, Gardiner Jr WC, Stein SE. Mechanism of soot formation in acetylene-oxygen mixtures. Combust Sci Technol 1986;50: 79–115.
[143] Appel J, Bockhorn H, Frenklach M. Kinetic modeling of soot formation with detailed chemistry and physics: laminar premixed flames of C_2 hydrocarbons. Combust Flame 2000;121:122–36.

[144] Stein SE. On the high temperature chemical equilibria of polycyclic aromatic hydrocarbons. J Phys Chem 1978;82:566–71.
[145] Stein SE, Fahr A. High-temperature stabilities of hydrocarbons. J Phys Chem 1985;89:3714–25.
[146] Frenklach M, Wang H. Detailed modeling of soot particle nucleation and growth. Proc Combust Inst 1991;23:1559–66.
[147] Frenklach M, Moriarty NW, Brown NJ. Hydrogen migration in polyaromatic growth. Proc Combust Inst 1998;27:1655–61.
[148] Moriarty NW, Brown NJ, Frenklach M. Hydrogen migration in the phenylethen-2-yl radical. J Phys Chem A 1999;103:7127–35.
[149] Miller JH, Herdman JD. Computational and experimental evidence for polynuclear aromatic hydrocarbon aggregation in flames. In: Bockhorn H, D'Anna A, Sarofim AF, Wang H, editors. Combustion generated fine carbonaceous particles (proceedings of an international workshop held in Villa Orlandi, Anacapri, May 13–16, 2007). KIT Scientifc Publishing; 2009. p. 259–76.
[150] Hwang JY, Chung SH. Growth of soot particles in counterflow diffusion flames of ethylene. Combust Flame 2001;125:752–62.
[151] Fenimore CP, Jones GW. Oxidation of soot by hydroxyl radicals. J Phys Chem 1967;71:593–7.
[152] Neoh KG, Howard JB, Sarofim AF. Soot oxidation in flames. In: Siegla DC, Smith GW, editors. Particulate carbon: formation during combustion. New York: Plenum Press; 1981. p. 261–82.
[153] Lighty JS, Romano V, Sarofim AF. Soot oxidation. In: Bockhorn H, D'Anna A, Sarofim AF, Wang H, editors. Combustion generated fine carbonaceous particles (proceedings of an international workshop held in Villa Orlandi, Anacapri, May 13–16, 2007). KIT Scientifc Publishing; 2009. p. 523–36.
[154] Richter H, Howard JB. Formation of polycyclic aromatic hydrocarbons and their growth to soot—a review of chemical reaction pathways. Prog Energy Combust 2000;26:565–608.
[155] Kennedy IM. Models of soot formation and oxidation. Prog Energy Combust 1997;23:95–132.
[156] Mansurov ZA. Soot formation in combustion processes (review). Combust Explo Shock Waves 2005;41:727–44.
[157] Amann CA, Siegla DC. Diesel particulates—what they are and why. Aerosol Sci Technol 1982;1:73–101.
[158] Feng T. Numerical modeling of soot and NO_x formation in non-stationary diesel flames with complex chemistry. Ph.D. thesis; Chalmers University of Technology, 2003.
[159] Smith GW. Kinetic aspects of diesel soot coagulation. Society of automotive engineers (SAE) paper 820466; 1982.
[160] Eckbreth AC. Laser diagnostics for combustion temperature and species. 1st ed. Cambridge: Abacus Press; 1988.
[161] Fristrom RM. Probe measurements in laminar combustion systems. In: Goulard R, editor. Combustion measurements: modern techniques and instrumentation. New York: Academic Press; 1976. p. 287–317.
[162] Bilger RW. Probe measurements in turbulent combustion. In: Goulard R, editor. Combustion measurements: modern techniques and instrumentation. New York: Academic Press; 1976. p. 333–51.
[163] McGregor WK. In situ optical versus probe sampling measurement of NO concentration in jet engine exhaust. In: Goulard R, editor. Combustion measurements: modern techniques and instrumentation. New York: Academic Press; 1976. p. 325–32.
[164] Society of Automotive Engineers (SAE). Snap acceleration smoke test procedure for heavy-duty powered vehicles, vol. J1667; 1996.
[165] Society of Automotive Engineers (SAE). Aircraft gas turbine engine exhaust smoke measurements. Aerospace recommended practice ARP1179A; 1970.
[166] Roberts R. Particulate measurement in the exhaust of gas turbine engines. In: Goulard R, editor. Combustion measurements: modern techniques and instrumentation. New York: Academic Press; 1976. p. 361–3.
[167] Society of Automotive Engineers (SAE). Aircraft exhaust nonvolatile particle matter measurement method development. Aerospace information report, SAE Air 6037; 2010.
[168] Liscinsky DS, Hollick HH. Effect of particle sampling technique and transport on particle penetration at the high temperature and pressure conditions found in gas turbine combustors and engines. NASA contractor report, NASA/CR-2010-NNC07CB03C; 2010.
[169] Clark HR, Stawicki RP, Smyth IP, Potkay E. Collection and characterization of soot from an optical fiber preform torch. J Am Ceram Soc 1990;73:2987–91.
[170] Saito K, Gordon AS, Williams FA, Stickle WF. A study of the early history of soot formation in various hydrocarbon diffusion flames. Combust Sci Technol 1991;80:103–19.
[171] Dobbins RA, Megaridis CM. Morphology of flame-generated soot as determined by thermophoretic sampling. Langmuir 1987;3:254–9.
[172] Chandler MF, Teng Y, Köylü ÜÖ. Diesel engine particulate emissions: a comparison of mobility and microscopy size measurements. Proc Combust Inst 2007;31:2971–9.
[173] Crookes RJ, Sivalingam G, Nazha MAA, Rajakaruna H. Prediction and measurement of soot particulate formation in a confined diesel fuel spray-flame at 2.1 MPa. Int J Therm Sci 2003;42:639–46.
[174] Shaddix CR, Palotás ÁB, Megaridis CM, Choi MY, Yang NYC. Soot graphitic order in laminar diffusion flames and a large-scale JP-8 pool fire. Int J Heat Mass Transfer 2005;48:3604–14.
[175] Fang TC, Megaridis CM, Sowa WA, Samuelsen GS. Soot morphology in a liquid-fueled, swirl-stabilized combustor. Combust Flame 1998;112:312–28.
[176] Hu B, Köylü ÜÖ. Size and morphology of soot particulates sampled from a turbulent non-premixed acetylene flame. Aerosol Sci Technol 2004;38:1009–18.
[177] Yang B, Hu B, Köylü ÜÖ. Mean soot volume fractions in turbulent hydrocarbon flames: a comparison of sampling and laser measurements. Combust Sci Technol 2005;177:1603–26.
[178] Kim CH, El-Leathy AM, Xu F, Faeth GM. Soot surface growth and oxidation in laminar diffusion flames at pressures of 0.1–1.0 atm. Combust Flame 2004;136:191–207.
[179] Köylü ÜÖ, McEnally CS, Rosner DE, Pfeferle LD. Simultaneous measurements of soot volume fraction and particle size/microstructure in flames using a thermophoretic sampling technique. Combust Flame 1997;110:494–507.
[180] Lin KC, Sunderland PB, Faeth GM. Soot nucleation and growth in acetylene air laminar coflowing jet diffusion flames. Combust Flame 1996;104:369–75.
[181] Megaridis CM, Dobbins RA. Soot aerosol dynamics in a laminar ethylene diffusion flame. Proc Combust Inst 1989;22:353–62.
[182] Megaridis CM, Dobbins RA. Morphological description of flame-generated materials. Combust Sci Technol 1990;71:95–109.
[183] Sunderland PB, Köylü ÜÖ, Faeth GM. Soot formation in weakly buoyant acetylene-fueled laminar jet diffusion flames burning in air. Combust Flame 1995;100:310–22.
[184] Sunderland PB, Faeth GM. Soot formation in hydrocarbon/air laminar jet diffusion flames. Combust Flame 1996;105:132–46.
[185] Vander Wal RL. A TEM methodology for the study of soot particle structure. Combust Sci Technol 1997;126:333–57.
[186] Zhang J, Megaridis CM. Soot microstructure in steady and flickering laminar methane/air diffusion flames. Combust Flame 1998;112:473–84.
[187] Snelling DR, Liu F, Smallwood GJ, Gülder ÖL. Determination of the soot absorption function and thermal accommodation coefficient using low-fluence LII in a laminar coflow ethylene diffusion flame. Combust Flame 2004;136:180–90.
[188] Modest MF. Radiative heat transfer. 2nd ed. Boston: Academic Press; 2003.
[189] Snelling DR, Thomson KA, Smallwood GJ, Gülder ÖL. Two-dimensional imaging of soot volume fraction in laminar diffusion flames. Appl Opt 1999;38:2478–85.
[190] Thomson KA, Matthew RJ, Snelling DR, Smallwood GJ. Diffuse-light two-dimensional line-of-sight attenuation for soot concentration measurements. Appl Opt 2008;47:694–703.
[191] Thomson KA. Soot formation in annular non-premixed laminar flames of methane–air at pressures of 0.1 to 4.0 MPa. Ph.D. thesis; University of Waterloo, 2004.
[192] Karataş AE. Soot formation in co-flow and counterflow laminar diffusion flames of fuel mixtures. Master's thesis; University of Toronto, 2010.
[193] Hall RJ, Bonczyk PA. Sooting flame thermometry using emission/absorption tomography. Appl Opt 1990;29:4590–8.
[194] Klassen M, Gore JP, Sivathanu YR. Radiative heat feedback in a toluene pool fire. Proc Combust Inst 1992;24:1713–9.
[195] Choi MY, Hamins A, Mulholland GW, Kashiwagi T. Simultaneous optical measurement of soot volume fraction and temperature in premixed flames. Combust Flame 1994;99:174–86.
[196] Klassen M, Gore JP. Temperature and soot volume fraction statistics in toluene-fired pool fires. Combust Flame 1993;93:270–8.
[197] De Iuliis S, Barbini M, Benecchi S, Cignoli F, Zizak G. Determination of the soot volume fraction in an ethylene diffusion flame by multiwavelength analysis of soot radiation. Combust Flame 1998;115:253–61.
[198] Snelling DR, Thomson KA, Smallwood GJ, Gülder ÖL, Weckman EJ, Fraser RA. Spectrally resolved measurement of flame radiation to determine soot temperature and concentration. AIAA J 2002;40:1789–95.
[199] Huang Q, Wang F, Liu D, Ma Z, Yan J, Chi Y, et al. Reconstruction of soot temperature and volume fraction profiles of an asymmetric flame using stereoscopic tomography. Combust Flame 2009;156:565–73.
[200] Santoro RJ, Shaddix CR. Laser induced incandescence. In: Kohse-Höinghaus K, Jefries JB, editors. Applied combustion diagnostics. New York: Taylor & Francis; 2002. p. 252–86.
[201] Zhao H, Ladommatos N. Optical diagnostics for soot and temperature measurement in diesel engines. Prog Energy Combust 1998;24:221–55.
[202] Schulz C, Kock BF, Hofmann M, Michelsen H, Will S, Bougie B, et al. Laser induced incandescence: recent trends and current questions. Appl Phys B Lasers Opt 2006;83:333–54.
[203] Bougie B, Tulej M, Dreier T, Dam NJ, ter Meulen JJ, Gerber T. Optical diagnostics of diesel spray injections and combustion in a high pressure high-temperature cell. Appl Phys B Lasers Opt 2005;80:1039–45.
[204] Crua C, Kennaird DA, Heikal MR. Laser induced incandescence study of diesel soot formation in a rapid compression machine at elevated pressures. Combust Flame 2003;135:475–88.
[205] Dreier T, Bougie B, Dam NJ, Gerber T. Modeling of time-resolved laser induced incandescence transients for particle sizing in high pressure spray combustion environments: a comparative study. Appl Phys B Lasers Opt 2006;83:403–11.
[206] Ryser R, Gerber T, Dreier T. Soot particle sizing during high pressure diesel spray combustion via time-resolved laser induced incandescence. Combust Flame 2009;156:120–9.
[207] Bougie B, Ganippa LC, van Vliet AP, Meerts WL, Dam NJ, ter Meulen JJ. Laser induced incandescence particle size measurements in a heavy-diesel engine. Combust Flame 2006;145:635–7.

[208] Bougie B, Ganippa LC, van Vliet AP, Meerts WL, Dam NJ, ter Meulen JJ. Soot particulate size characterization in a heavy-duty diesel engine for different engine loads by laser induced incandescence. Proc Combust Inst 2007;31:685–91.
[209] Hofmann M, Bessler WG, Schulz C, Jander H. Laser induced incandescence for soot diagnostics at high pressures. Appl Opt 2003;42:2052–62.
[210] Hofmann M, Kock BF, Dreier T, Jander H, Schulz C. Laser induced incandescence for soot-particle sizing at elevated pressure. Appl Phys B Lasers Opt 2008;90:629–39.
[211] Liu F, Daun KJ, Snelling DR, Smallwood GJ. Heat conduction from a spherical nano-particle: Status of modeling heat conduction in laser induced incandescence. Appl Phys B Lasers Opt 2006;83:355–82.
[212] Beyer V, Greenhalgh DA. Laser induced incandescence under high vacuum conditions. Appl Phys B Lasers Opt 2006;83:455–67.
[213] Liu F, Daun KJ, Beyer V, Smallwood GJ, Greenhalgh DA. Some theoretical considerations in modeling laser induced incandescence at low-pressures. Appl Phys B Lasers Opt 2007;87:179–91.
[214] Thomson KA, Snelling DR, Smallwood GJ, Liu F. Laser induced incandescence measurements of soot volume fraction and effective particle size in a laminar co-annular non-premixed methane/air flame at pressures between 0.5–4.0 MPa. Appl Phys B Lasers Opt 2006;83:469–75.
[215] Tsurikov MS, Geigle KP, Krüger V, Schneider-Kühnle Y, Stricker W, Lückerath R, et al. Laser-based investigation of soot formation in laminar premixed flames at atmospheric and elevated pressures. Combust Sci Technol 2005;177:1835–62.
[216] Liu F, Thomson KA, Smallwood GJ. Effects of soot absorption and scattering on LII intensities in laminar coflow diffusion flames. J Quant Spectrosc Radiat Transfer 2008;109:337–48.
[217] Liu F, Snelling DR, Smallwood GJ. Numerical study of temperature and incandescence intensity of nanosecond pulsed-laser heated soot particles at high pressures. IMECE2005–81322; 2005.
[218] Snelling DR, Smallwood GJ, Liu F, Gülder ÖL, Bachalo WD. A calibration-independent laser induced incandescence technique for soot measurement by detecting absolute light intensity. Appl Opt 2005;44:6773–85.
[219] Charwath M, Suntz R, Bockhorn H. Constraints of two-colour TiRe-LII at elevated pressures. Appl Phys B Lasers Opt 2011;104:427–38.
[220] Bone WA, Townend DTA. Flame and combustion in gases. 1st ed. London: Longmans; 1927.
[221] McArragher JS, Tan KJ. Soot formation at high pressures: a literature review. Combust Sci Technol 1972;5:257–61.
[222] Townend DTA. Gaseous combustion at high pressures. Part VIII. The explosion of methane with up to its own volume of oxygen at initial pressures up to 150 atmospheres. Proc R Soc Lond A 1927;116:637–63.
[223] Bell J. Spectrographic studies of the explosive combustion of methane. Proc R Soc Lond A 1937;158:429–54.
[224] Smith ECW. The emission spectrum of hydrocarbon flames. Proc R Soc Lond A 1940;174:110–25.
[225] Roper FG, Smith C, Cunningham AC. The prediction of laminar jet diffusion flame sizes: Part II. Experimental verification. Combust Flame 1977;29:227–34.
[226] Schalla RL, McDonald GE. Mechanism of smoke formation in diffusion flames. Proc Combust Inst 1955;5:316–24.
[227] Schalla RL, Clark TP, McDonald GE. Formation and combustion of smoke in laminar flames. Tech. Rep. 1186; NACA; 1954.
[228] Fenimore CP, Jones GW, Moore GE. Carbon formation in quenched flat flames at 1600°K. Proc Combust Inst 1957;6:242–7.
[229] Macfarlane JJ, Holderness FH, Whitcher FSE. Soot formation rates in premixed C_5 and C_6 hydrocarbon–air flames at pressures up to 20 atmospheres. Combust Flame 1964;8:215–29.
[230] Burke SP, Schumann TEW. Diffusion flames. Proc Combust Inst 1948;1:2–11.
[231] Flower WL, Bowman CT. Measurements of the effect of elevated pressure on soot formation in laminar diffusion flames. Combust Sci Technol 1984;37:93–7.
[232] Flower WL, Bowman CT. Measurements of the structure of sooting laminar diffusion flames at elevated pressures. Proc Combust Inst 1985;20:1035–44.
[233] Flower WL. The effect of elevated pressure on the rate of soot production in laminar diffusion flames. Combust Sci Technol 1986;48:31–43.
[234] Glassman I. Sooting laminar diffusion flames: effect of dilution, additives, pressure, and microgravity. Proc Combust Inst 1998;27:1589–96.
[235] ASTM Standard D1322–08. Standard test method for smoke point of kerosene and aviation turbine fuel. ASTM International; 2008.
[236] Gülder ÖL. Influence of hydrocarbon fuel structural constitution and flame temperature on soot formation in laminar diffusion flames. Combust Flame 1989;78:179–94.
[237] Schug KP, Manheimer-Timnat Y, Yaccarino P, Glassman I. Sooting behavior of gaseous hydrocarbon diffusion flames and the influence of additives. Combust Sci Technol 1980;22:235–50.
[238] Glassman I, Yaccarino P. The effect of oxygen concentration on sooting diffusion flames. Combust Sci Technol 1981;24:107–14.
[239] Glassman I, Yaccarino P. The temperature effect in sooting diffusion flames. Proc Combust Inst 1981;18:1175–83.
[240] Markstein GH. Relationship between smoke point and radiant emission from buoyant turbulent and laminar diffusion flames. Proc Combust Inst 1985;20:1055–61.
[241] Kent JH. A quantitative relationship between soot yield and smoke point measurements. Combust Flame 1986;63:349–58.
[242] Markstein GH. Radiant emission and smoke points for laminar diffusion flames of fuel mixtures. Proc Combust Inst 1987;21:1107–14.
[243] Lin KC, Faeth GM. Hydrodynamic suppression of soot emissions in laminar diffusion flames. J Propul Power 1996;12:10–7.
[244] Gohari Darabkhani H, Bassi J, Huang HW, Zhang Y. Fuel effects on diffusion flames at elevated pressures. Fuel 2009;88:264–71.
[245] Gohari Darabkhani H, Zhang Y. Impact of pressure and fuel flow rate on flame dynamics in a high pressure combustor. CEAS European Air and Space Conference, 2009.
[246] Gohari Darabkhani H, Zhang Y. Methane diffusion flame dynamics at elevated pressures. Combust Sci Technol 2010;182:231–51.
[247] Davis RW, Moore EF, Santoro RJ, Ness JR. Isolation of buoyancy effects in jet diffusion flame experiments. Combust Sci Technol 1990;73:625–35.
[248] Gohari Darabkhani H, Zhang Y. Pressure effects on structure and temperature field of laminar diffusion flames. 48th AIAA aerospace sciences meeting; 2010.
[249] Northrup SA, Groth CPT. Solution of laminar diffusion flames using a parallel adaptive mesh refinement algorithm. 43rd AIAA aerospace sciences meeting; 2005.
[250] Charest MRJ, Groth CPT, Gülder ÖL. Numerical prediction of sooting laminar diffusion flames using adaptive mesh refinement. Proceedings of the sixth U.S. national combustion meeting; 2009.
[251] Smith GP, Golden DM, Frenklach M, Moriarty NW, Eiteneer B, Goldenberg M, et al. GRI 3.0, http://www.me.berkeley.edu/gri_mech/; 2002.
[252] Mandatori PM. Soot formation in ethane–air coflow laminar diffusion flames at elevated pressures. Master's thesis; University of Toronto, 2006.
[253] Calcote HF, Manos DM. Effect of molecular structure on incipient soot formation. Combust Flame 1983;49:289–304.
[254] Olson DB, Pickens JC, Gill RJ. The effects of molecular structure on soot formation II. Diffusion flames. Combust Flame 1985;62:43–60.
[255] Kock BF, Eckhardt T, Roth P. In-cylinder sizing of diesel particles by time-resolved laser induced incandescence (TR-LII). Proc Combust Inst 2002;29:2775–81.
[256] Neer A, Köylü ÜÖ. Effect of operating conditions on the size, morphology, and concentration of submicrometer particulates emitted from a diesel engine. Combust Flame 2006;146:142–54.
[257] Moss JB, Stewart CD, Syed KJ. Flowfield modelling of soot formation at elevated pressure. Proc Combust Inst 1989;22:413–23.
[258] Charest MRJ, Groth CPT, Gülder ÖL. Effects of gravity and pressure on laminar coflow methane–air diffusion flames at pressures from 1 to 60 atmospheres. Combust Flame 2011;158:860–75.
[259] Charest MRJ, Groth CPT, Gülder ÖL. A numerical study on the effects of pressure and gravity in laminar ethylene diffusion flames. Combust Flame 2011;158:1933–45.